FORCES BETWEEN MINERALS AND BIOLOGICAL SURFACES IN AQUEOUS SOLUTION

Treavor A. Kendall[1] and Steven K. Lower[2]

[1]Harvard University, Division of Engineering and Applied Sciences, 40 Oxford St., Cambridge, MA 02138, USA
[2]Department of Geological Sciences & School of Natural Resources, The Ohio State University, 275 Mendenhall Laboratory, 125 South Oval Mall, Columbus, Ohio 43210, USA, Email: lower.9@osu.edu

Advances in Agronomy, Volume 82

0065-2113/03 $35.00

At the most fundamental level, intermolecular forces (e.g., van der Waals, electrostatic, solvation, steric) control interactions between biological molecules and mineral surfaces. These are forces with magnitudes of piconewtons to nanonewtons, which operate in a space that is on the order of nanometers. We have used force microscopy to quantitatively probe forces, energies, and distances between crystal surfaces and living microbial cells or biological molecules in their native state. The systems we have studied include those involving: *Escherichia coli*, *Shewanella oneidensis*, siderophores, muscovite, goethite, and/or diaspore, in aqueous solutions of varying composition. Direct force measurements at the organic–inorganic interface have been interpreted with theoretical models describing interfacial forces, adhesion, and molecular dynamic calculations. A new perspective on bacterium–mineral interactions is emerging from these studies. We have discovered a world that operates under a very different set of principles than macroscopic bodies. A world where the intermolecular force, rather than gravitational attraction, is the preeminent force controlling the evolution of processes at the bacterium–mineral interface.

I. INTRODUCTION — FORCES IN NATURE

The bacterium–mineral interface is ubiquitous near the surface of the Earth. As many as 97% of the $\sim 10^{30}$ prokaryotes on Earth live in close proximity to minerals in soil, marine, and terrestrial subsurface environments (Whitman *et al.*, 1998). As we will show in this manuscript, the fundamental forces at this interface are very small, seemingly insignificant. This review will provide evidence that forces on the order of nanonewtons (10^{-9} N) to piconewtons (10^{-12} N) dominate the properties/processes at bacterium–mineral and biomolecule–mineral interfaces. For comparison, there is ~ 0.2 nN of gravitational attraction between a person (50 kg) and the paper (5 g) upon which these words are written. Despite their small magnitude, these forces are at the heart of all interactions between biologically produced polymers and mineral surfaces in nature.

It is now well established that there are four fundamental forces in nature: the strong and weak nuclear forces, the gravitational interaction, and electromagnetic forces, which are the source of all intermolecular forces (Israelachvili, 1992). Because the first two (i.e., nuclear forces) have a range of action that is less than 10^{-5} nm (Israelachvili, 1992), we need not consider these for interactions between biological molecules, microbial cells, and/or mineral surfaces. The question then becomes, under what conditions do gravitational forces or electromagnetic forces (more specifically, intermolecular forces) dominate bacteria–mineral or biomolecule–mineral interactions?

In nature, living organisms exist in communities that are in contact with one another, in contact with mineral surfaces, and they are also in contact with the surface of the Earth (i.e., the upper crust). For simplicity, let us define a particular species of organism as a spherical particle (having a density of water) with a unique size or radius. Each species may interact with one another and/or the Earth. In both instances, there is a force of gravitational attraction at each interface. Figure 1 reveals that the gravitational attraction is much greater between the Earth and a particle of a given size (e.g., $\sim 4 \times 10^{-5}$ N for a 1 mm particle) relative to the gravitational attraction between two particles of the same given size (e.g., $\sim 3 \times 10^{-16}$ N between two 1 mm particles). Also shown on this figure is a theoretical prediction for another type of attractive force, the so-called van der Waals force. This intermolecular force was determined using Eq. (1) (see below) to describe the attraction between two similar objects of equal size in contact with one another. For example, two identical 1 mm (radius) particles are

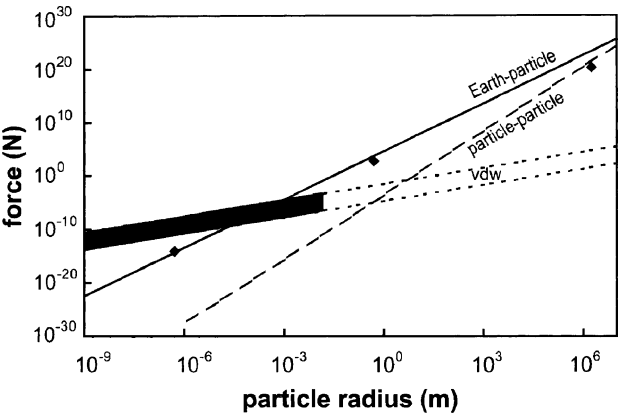

Figure 1 Log–log plot of the theoretical forces describing (1) gravitational attraction between a particle and the Earth (solid "Earth-particle" line), (2) gravitational attraction between two particles of the same size (dashed "particle-particle" line), and (3) van der Waals attraction between two particles of the same size (dashed "vdw" lines). In all instances the particles are assumed to be in "contact" with the Earth (for 1) or another particle (for 2 and 3). For gravitational attraction, mass was determined by assuming each particle was a solid homogeneous sphere with a density of 1 g cm^{-3}, and contact was defined as the radius of the Earth (~6.4×10^6 m radius; "Earth-particle" interaction) or the sum of the radii of two interacting particles ("particle-particle" interaction). The shaded region outlines the boundaries of the expected van der Waals force using values for Hamaker constant of 10^{-20} to 10^{-21} J, which is appropriate for biological and inorganic phases (Israelachvili, 1992; Leckband and Israelachvili, 2001; Vigeant *et al*., 2002), and defining "contact" as an effective separation between particles of ~0.2 (for one hydration layer) to 2 nm, according to Israelachvili (1992) and Leckband and Israelachvili (2001). Only the magnitudes of the forces are shown. By convention, attractive forces (shown here) are negative. For reference, the three diamond symbols represent gravitational forces between the Earth (~10^{24} kg) and each of three bodies (from left to right): a bacterium (10^{-15} kg), a human (50 kg), or the moon (10^{22} kg).

expected to have an attractive, adhesion force at contact (due solely to the van der Waals force) equal to $\sim 3 \times 10^{-5}$ N (Hamaker constant $= 10^{-20}$ J; effective separation $= 0.165$ nm, i.e., the "universal" cut-off separation, Israelachvili, 1992). This force magnitude is approximately the same as the gravitational force between the Earth's surface and one of these 1 mm particles. While it is debatable whether the van der Waals force applies in the same manner to both a particle of the size of an atom and an object of the size of the moon, the predictions shown in Fig. 1 for objects smaller than ~ 1 cm are in agreement with others (e.g., Israelachvili, 1992). Consequently, the force of gravity may dominate the interactions between macroscopic bodies (e.g., plants and animals), but intermolecular forces (e.g., van der Waals and others, see below) are the prevailing forces with which microscopic bacteria must contend. This is particularly true when one considers that the van der Waals force is significantly weaker and shorter range than other intermolecular forces, such as electrostatic and hydrophobic interactions as discussed below.

II. FUNDAMENTAL FORCES AT THE INTERFACE OF BIOLOGICAL PARTICLES AND INORGANIC SURFACES

"All intermolecular forces are essentially electrostatic in origin" (page 11, Israelachvili, 1992). In theory, classical electrostatics could be used to calculate intermolecular forces if one could determine the spatial distribution of the electron cloud by solving the Schrödinger equation (Israelachvili, 1992). Unfortunately this is challenging for even simple atomic interactions in vacuum, never mind molecular or organism scale interactions between different functional groups on bacteria and minerals in water. For this reason, it is useful to classify four types of intermolecular forces that are expected to dominate the bacterium–mineral and biomolecule–mineral interfaces. These include the van der Waals force, electrostatic forces, solvation interactions, and steric or entropic forces (Israelachvili and McGuiggan, 1988). The reader is referred to a number of excellent reviews on these types of forces (e.g., Israelachvili and McGuiggan, 1988; Butt *et al*., 1995; Leckband and Israelachvili, 2001). This review will touch on all four types of intermolecular forces, although the van der Waals and electrostatic forces will be explored in more detail.

A. The van der Waals Force

The van der Waals force, like the force of gravity, acts between all particles (Israelachvili, 1992). It is quantum mechanical in origin and arises because of

the time dependent fluctuations in the electric dipole moment of a particle as it comes into contact with other particles nearby. Even nonpolar particles, which have a time averaged dipole moment of zero, have instantaneous dipoles due to the movement of electrons relative to protons in a nucleus. Dipoles generate an electric field that polarizes adjacent particles and gives rise to an instantaneous force between neighboring particles. Two terms describe the van der Waals force: the first polarization potential, which represents the energy necessary to ionize an atom (i.e., a dipole moment due to interactions between electrons and protons *within* a single particle); and the so-called dispersion term, which describes the dipole induced interactions between two or more atoms (Israelachvili, 1992). Because the dispersion term dominates the van der Waals force, it is sometimes referred to as (London) dispersion forces (Butt *et al*., 1995).

The van der Waals force has an inverse power law dependence on the separation between two particles. For atoms and small molecules the van der Waals force is $\sim D^{-7}$, where D is the separation distance between particles. It can be attractive or repulsive (e.g., it is always attractive between two similar particles immersed in a third liquid) and is described in terms of the Hamaker constant (H_a), which depends upon the refractive indices and dielectric constants of the interacting particles and intervening media (see Israelachvili, 1992). Hamaker constants are in the order of 10^{-20} to 10^{-21} J, for biological cells or molecules interacting with themselves or minerals across an aqueous solution (Ducker *et al*., 1991; Butt *et al*., 1995; Ong *et al*., 1999; Bhattacharjee *et al*., 2000; Leckband and Israelachvili, 2001; Vigeant *et al*., 2002).

For simple geometries, the forces between atoms or molecules can be assumed to be additive (Israelachvili, 1992; Butt *et al*., 1995) such that equations can be derived for larger particles (e.g., organic and inorganic surfaces). Two commonly encountered geometric configurations include interactions between two spheres or a sphere and a flat surface, both of which are given by Israelachvili (1992), Butt *et al*. (1995) and Leckband and Israelachvili (2001):

$$F(D) = \frac{-H_{\mathrm{a}} R_x}{6D^2} \tag{1}$$

where H_{a} is the Hamaker constant (J), D is the separation distance (m) between the two spheres or a sphere and a plane, and R_x (m) equals the radius of the sphere for the sphere–plane configuration, or it is equal to $(R_1 R_2/(R_1+R_2))$ for the interaction between two spheres of radius R_1 and R_2. A positive Hamaker constant indicates attraction (negative force sign).

B. The Electrostatic Force

The electrostatic force arises through a variety of mechanisms leading to the development of surface charge (e.g., see Sposito, 1989). Water, which has a high

dielectric constant, causes the dissociation of surface functional groups. These functional groups display protonation/deprotonation reactions that are dependent upon pH. For example, in water, silanol groups on a silica surface undergo the following reaction: $>\mathrm{Si\,OH} = >\mathrm{Si\,O^-} + \mathrm{H^+}$. Similar acid–base reactions take place on carboxylic groups, amine groups, and other reactive moieties on biological molecules and inorganic surfaces. Hence, many inorganic and biological surfaces develop a charge that is dependent upon pH. Other factors such as the adsorption of charged ions and presence of permanent structural charge (e.g., for clays) are additional contributors to surface charge. The overall charge on a surface is balanced by the dissolved counterions in solution, which are attracted to the surface by its electric field and dispersed such that they (i.e., the counterions) increase entropy (Butt *et al*., 1995). This creates the so-called electric double-layer around surfaces immersed in aqueous solution (Stumm, 1992). When two charged surfaces approach one another, the electric double-layers are perturbed resulting in an electrostatic interaction. This interaction may be attractive (if surfaces are of opposite charge) or repulsive (if surfaces are similarly charged).

The electrostatic force varies exponentially with the distance between particles. It depends strongly upon the surface charge densities of the interacting particles and the ionic strength of the intervening solution. Similar to the van der Waals force (see above) equations can be derived to describe the electrostatic force for various geometric configurations. The model for electrostatic forces between two spheres or a sphere and flat surface is (Butt *et al*., 1995; Muller and Engel, 1997; Leckband and Israelachvili, 2001):

$$F(D) = \frac{4\pi\sigma_1\sigma_2 R_x}{\varepsilon\varepsilon_0\kappa} \mathrm{e}^{-\kappa D} \tag{2}$$

where σ is the surface charge density ($\mathrm{C\,m^{-2}}$) of particles 1 and 2, ε is the dielectric constant of water (78.54 at 298 K), ε_0 is the permittivity of free space (8.854×10^{-12} $\mathrm{C^2\,J^{-1}\,m^{-1}}$), R_x and D are defined as above. The Debye length ($1/\kappa$) describes the thickness of the diffuse double-layer of counterions that surrounds charged particles in solution. The Debye length depends upon the valence and concentration (c, $\mathrm{mol\,L^{-1}}$) of the electrolyte. For monovalent electrolytes (e.g., NaCl) at a temperature of 298 K, the Debye length (in nm) = $0.304/(c)^{1/2}$; for 1:2 or 2:1 electrolytes (e.g., $\mathrm{CaCl_2}$) it is $0.174/(c)^{1/2}$; for 2:2 electrolytes it is $0.152/(c)^{1/2}$ (Muller and Engel, 1997). In many instances, it is easier to determine a particle's surface potential as opposed to surface charge. The Graham equation can be used to relate these two parameters according to (Stumm, 1992),

$$\sigma = \sqrt{8RT\varepsilon\varepsilon_0 c \times 10^3} \times \sinh\left(\frac{z\psi F}{2RT}\right) \tag{3}$$

where R is the gas constant (8.314 $\mathrm{J\,mol^{-1}\,K^{-1}}$), T is the temperature (K), z is the valence of ions in solution, ψ is the surface potential (V), and F is the Faraday constant (96,490 $\mathrm{C\,mol^{-1}}$). A potential measured across an interface

contains contributions from at least two layers, the so-called Stern layer and the "diffuse" layer (see Stumm, 1992). Techniques such as streaming potential and electrophoresis are commonly used to determine a particle's zeta potential, which is used as a proxy for surface potential. However, the zeta potential probably represents only the "diffuse" double-layer, which is lower than the true surface potential (Stumm, 1992). Leckband and Israelachvili (2001) describe the differences for surfaces that are assumed to have a constant surface charge *versus* those that are assumed to have a constant surface potential. Interactions at constant surface charge are expected to occur when surface ionizable groups are fully dissociated and remain as such for all separations (D). This may be true when the pH of a solution is much greater than the pK value(s) of a particular protonation/deprotonation reaction(s). In instances where surface functional groups are not fully ionized but in equilibrium with solution ions, interactions at constant potential are expected to occur. In this latter case, as two surfaces come together (i.e., very small D) the intervening concentration of solution ions increases locally such that some solution ions bind to the surface thereby reducing that surface's density of charged sites (Leckband and Israelachvili, 2001). For many instances, this distinction influences the interaction only at small separations where these two conditions define the boundaries of the expected electrostatic force.

C. The Solvation Force

The origin, theory, and force–distance relationships of the remaining two force classes — solvation and steric — are indefinite compared to the forces discussed above. Much work remains to be done before solvation and steric forces can be appreciated to the same extent as the van der Waals and electrostatic forces. However, it is well established that the models developed for the van der Waals and electrostatic forces, which treat the intervening solution as a continuum, break down when two particles or surfaces are within a few nanometers (Butt *et al*., 1995; Leckband and Israelachvili, 2001). At such close separations, solvation forces may dominate because the solvent (e.g., water) takes on a more ordered structure. Steric forces may also come into play for surfaces with polymers (e.g., biological cells or particles). Our discussion of solvation and steric forces will be more qualitative however, because general force laws (such as those described above) are relatively sparse for these latter two force classes.

Solvation forces (also called hydration or structural forces when the solvent is water) seem to be the result of interactions of solvent molecules with themselves (e.g., in a confined space between two surfaces) or interactions between solvent molecules and a surface (e.g., the orientation of water molecules at the interface of a strongly hydrophilic surface). As two surfaces approach one another the

intervening liquid ceases to behave as a structureless media resulting in a force that can be attractive, repulsive, or oscillatory (Butt *et al*., 1995). These forces can be further subdivided into those that result from solvent–solvent, solvent–surface, and surface–surface interactions (Israelachvili and McGuiggan, 1988).

For two rigid crystalline surfaces at short-range (<2 nm for water), water molecules interact with themselves such that they take on a semi-discrete layering or structure, which causes the "structural" forces between the interacting surfaces to oscillate between attraction and repulsion with a periodicity equal to the molecular dimension of water (Leckband and Israelachvili, 2001). Between surfaces with polymers, water cannot form well-defined layers because headgroups on lipids, for example, are "rough" on the scale of a water molecule (Israelachvili, 1992), and macromolecules in surfaces are thermally mobile (Beveridge, 1999). Consequently, any repulsion is smeared out and takes on a monotonic component (Israelachvili, 1992). For strongly hydrophilic surfaces in aqueous solution, there is a strong solvent–surface interaction that leads to the formation of hydration shells. These ordered water molecules within the "shell" generate an electric field that impinges upon another surface as two particles approach to within a few nanometers of one another (Israelachvili and McGuiggan, 1988). For example, water molecules may associate with two, adjacent hydrophillic surfaces such that the water's hydrogens are oriented towards each surface (attracted via hydrogen bonds) and the water oxygens are exposed to the solution. This confers a negative character (from the lone pairs of the water's oxygens) to each surface, thereby generating a repulsive force. Conversely, the dipoles may complement one another forming an attractive force if water molecules are staggered on the two surfaces. This hydration force may extend outwards more than the oscillatory force discussed previously (Leckband and Israelachvili, 2001). Finally, for nonpolar surfaces that cannot bind to water molecules — the so-called hydrophobic surfaces (defined as those surfaces having a contact angle of 75–115° with water) — there is often a strong attractive force that extends to separations of tens of nanometers or greater (Leckband and Israelachvili, 2001). Hydrophobic forces can be significantly greater than the van der Waals force and may play an important role in interactions involving hydrophobic molecules and/or surfaces (Israelachvili and McGuiggan, 1988; Israelachvili, 1992).

D. The Steric Force and Bridging Polymers

The steric force affects surfaces that have flexible polymers extending out into solution (e.g., polysaccharides on biological cells). As two surfaces approach one another, the polymer chains become confined such that they are not free to move at random. This entropic confinement results in a repulsive force whose length scale is approximately equal to the radius of gyration of the polymer

(Butt *et al*., 1995), where the radius of gyration is proportional to the number of monomer segments raised to some power between 0.33 (for poor solvents) and 0.6 (for good solvents) (Leckband and Israelachvili, 2001). Approximations derived for the interaction between two flat surfaces reveal that this force depends on the surface coverage of the polymer and may take an exponential form (Israelachvili, 1992; Leckband and Israelachvili, 2001). At close separation, the magnitude of the steric force can be similar to that of the electrostatic force (Leckband and Israelachvili, 2001).

In some instances, surface-bound polymers may form an attractive interaction at close separation as the polymer forms a "bridge" between two particles or surfaces (Leckband and Israelachvili, 2001). The resulting adhesive bond may be very long range (i.e., extend well beyond the radius of gyration of the polymer) and resist separation when the surfaces are pulled apart (Jeppesen *et al*., 2001). While there is no general description for attractive bridging forces by polymers, the linkage of surfaces via a polymeric tether has been described by the so-called freely jointed chain (see e.g., Leckband and Israelachvili, 2001), or worm-like chain models (see e.g., Flory, 1989; Bustamante *et al*., 1994). In the case of the latter, the polymer is viewed as an elastic element and the force (F) needed to stretch the tethered polymer to a length x is:

$$F(x) = (k_{\mathrm{B}}T/b)[0.25(1 - x/L)^{-2} - 0.25 + x/L] \tag{4}$$

where k_{B} is the Boltzmann's constant, T is the temperature, b is the persistence length (i.e., length of the stiff segment or monomer of the chain), and L is the contour length (i.e., length of the completely stretched chain).

Polymer bridging is a phenomenon that crosses between the disciplines of colloidal science — which has historically tended to investigate intermolecular forces that dominate the interface between two rigid surfaces that are approaching one another — and adhesion science — which is interested in describing the contact between two surfaces and the forces necessary to pull them apart. While attractive intermolecular and intersurface forces (i.e., the four force classes discussed above) are responsible for adhesion events, real particles (e.g., bacteria and minerals) that make contact will also adhere to one another due to elastic or fluid-like deformation, which is an intrinsic and natural part of contact. There is a wealth of information on adhesion processes and theories including the Johnson–Kendall–Roberts (Johnson *et al*., 1971) and Derjaguin–Muller–Toporov (Derjaguin *et al*., 1975) theories, which relate the force required to pull two surfaces apart (i.e., the "pull off" force) to the surface energy, surface tension, or work of adhesion. Suffice it to say that surface energy (or tension or work) is determined from intermolecular forces between surfaces. For particles or surfaces that are incapable of forming hydrogen bonding (e.g., nonmetallic compounds), the surface energy can be related directly to the van der Waals force, where surface tension $\approx H_{\mathrm{a}}/2.1 \times 10^{-21}$ (Israelachvili, 1992). The surface

energies of more polar surfaces, which tend to be larger, are dependent upon van der Waals interactions, as well as an additional electrostatic-like term that relates surface energy to Lewis acid/base reactions (van Oss, 1993).

These four forces — van der Waals, electrostatic, solvation (hydration and hydrophobic), and steric — operate concurrently at the interfaces between microorganisms, biological molecules, and/or mineral surfaces (see Table 1). In some instances, one force may dominate at all separations. In other instances, there is a delicate balance such that each force dominates at its own length scale. These four force classes are often invoked to describe interactions as two surfaces approach one another. Two particles that are pulled apart may experience the same sign, magnitude, and range of forces that existed upon approach. However, there is often a notable hysteresis between the forces measured upon approach *versus* those that are observed upon retraction for soft biological particles and surfaces. This is due to the formation of adhesive bonds (e.g., see discussion of polymer bridges and adhesion, above) once contact has been established between surfaces. This review will provide examples that illustrate the various forces and force models discussed above as they pertain to interactions between biological and inorganic particles. Further, we will discuss the differences between those forces measured as surfaces

Table I
Summary of Physical Forces of Interaction Between Particles and/or Surfaces*

Type of interaction	Description
van der Waals	Force between all particles due to polarization; usually attractive; short-range
Electrostatic	Force between charged particles; attractive (for particles of opposite sign) or repulsive (for particles of similar sign); depends upon ionic strength of solution; short to long range
Solvation	Structural or hydration forces are typically repulsive due to sorbed water layers; short-range
	Hydrophobic force is attractive between nonpolar surfaces; short to long range
Steric	Typically a short-range, repulsive force associated with polymers; may be longer range, attractive force for "bridging" polymers.

*This review has followed the force characterization of Israelachvili (1988). Other force classes, such as hydrogen bonding or thermal fluctuations, may dominate when two particles or surfaces are very close. However, these other classes can often be described as a subset of electrostatic (for hydrogen bonding) or steric (for thermal fluctuations) interactions, according to Leckband and Israelachvili (2001). So-called specific interactions (e.g., ligand–receptor interactions) are typically a result of unique combinations of these four "non-specific" physical forces (Israelachvili, 1992).

come together relative to surfaces that are pulled apart. As a final point to this section, it should be noted that a force of interaction is related to energy (E) according to $F = -\mathrm{d}E/\mathrm{d}D$.

III. FORCE CURVE THEORY AND COLLECTING FORCE DATA

Force measurements attempt to capture interactions representing the electrostatic interplay between single molecules and atoms that are bound to a solid surface or exist as components of a solvated environment. Given the extraordinarily small dimensional (nanometer to angstrom) scale over which they operate, many challenges exist in capturing molecular level forces. This section reviews how force microscopy (or atomic force microscopy, AFM; also know as scanning probe microscopy) addresses these challenges, describes its operation and assesses how accurately the interactions are captured. Highlighted are some of the basic assumptions associated with force microscopy, while noting some of its advantages and limitations.

An AFM force probe consists of a tip attached to a flexible cantilever, which is modeled mechanically as a single harmonic oscillator. Forces exerted on the tip are registered as a spring-like deflection in the cantilever, which may be recorded with various detection systems, including electron tunneling (Binnig *et al*., 1986), interferomotery (Erlandsson *et al*., 1988; Rugar *et al*., 1989) and capacitance (Goddenhenrich *et al*., 1990). The following summarizes an optical lever collection system (Meyer and Amer, 1990) that is most commonly found in commercially available AFMs, including the widely used Veeco/Digital Instrument system. Here the deflection is typically recorded as a change in voltage resulting from the displacement of a laser spot that is reflected off the top of the cantilever and into a photodiode. Voltage (V) is translated into cantilever deflection (nm) using a detector sensitivity value (V nm^{-1}) that is equal to the slope of the line when the tip and sample are in contact (see region of contact in Fig. 2). Provided the sample stiffness is significantly higher than the cantilever (which is the case when probing mineral surfaces), there should be a 1:1 correlation between piezo movement and cantilever deflection once the (V to nm) conversion is made. Small deviations from an absolute slope equal to one may be an indication of detector drift, and can be corrected by dividing the deflection values by the slope (H. Skulason, personal communication). A slope less than one may also be an indication of a sample compliance that is less than the cantilever (which may be the case when making measurements on a cell), in which case alternative sensitivity determinations, such as the photodiode shift voltage method may be employed (D'Costa and Hoh, 1995; Lower *et al*., 2001b).

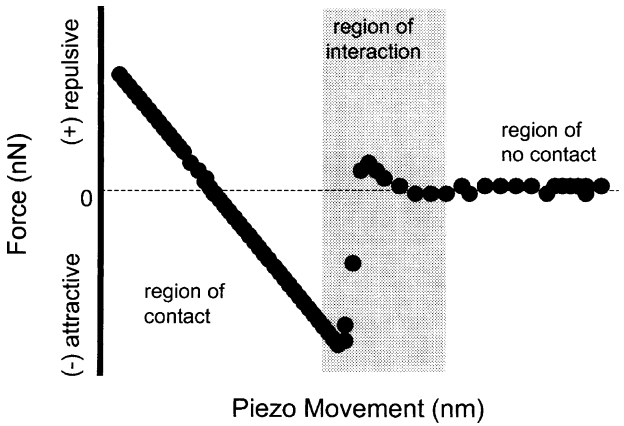

Figure 2 A typical force versus piezo movement plot showing three general regions — contact, interaction, and no contact. For clarity a single trace is shown (e.g. an approach curve); however, force plots with both approach and retraction traces are also common. In the region of no contact the tip and sample are separated at distances large enough that no interaction occurs. Hysteresis between the approach and retraction curve in the region of no contact may be a function of solution viscosity, or inelastic deformation of the cantilever. As the piezo advances the sample closer, the tip begins to "feel" the surface. In the example plot we see an initial repulsion followed by an attraction recorded as a sharp jump to contact that generates a minimum in the curve. Once in contact, the slope trace is typically constant as the cantilever is moving with the piezo. Information from this region may be used to determine detector sensitivity or elastic properties of the sample or tip.

Hooke's law, $F = -k_s d$, then allows conversion of cantilever deflection, d, into force, F, using the spring constant of the cantilever, k_s. Note that sign convention dictates that negative forces reflect attractive interactions and positive forces are repulsive.

A. Force–distance Curves, Capturing a Potential Force versus Separation Plot

Figure 2 shows a typical plot of force *versus* piezo movement. Note the x-axis represents relative piezo movement or an indexing of a sample's position relative to the cantilever (tip). It does not reflect tip-sample separation (discussed below). Three main components of the plot are identified: the regions of no contact, interaction and contact. Several sub-features are contained within each region including oscillations, subtle slope changes, linear and non-linear extensions, jumps to and from contact (Ducker *et al.*, 1992; Cappella and Dietler, 1999; Gergely *et al.*, 2001), which, in addition to providing reference points to register the force curve to an origin (discussed below), contain valuable information on the interaction between the tip and the surface, the nature of the intervening solution, tribology, adhesion, and elastic properties of the system.

The focus is now turned to the region of interaction, which is of primary interest when studying intermolecular forces at cell or biomolecule–mineral interfaces. Here a wealth of information on the charge character of a mineral surface or biomolecule; the nature and contour length of a polymer extending from a bacterium; DLVO forces (see below) and Debye lengths associated with a colloidal particle or cell; and the energy landscape and activation barriers of a bond are found. But first, to draw both qualitative and quantitative conclusions from forces of interaction, it is imperative to have an understanding of the mechanical constraints of what is recorded in this region using force microscopy using an AFM. To illustrate this we show a simple, short-range interaction potential for atomic scale particles (note, Part II concentrated mainly on larger particles and/or surfaces) described by the Lennard–Jones equation:

$$E(D) = -A/D^6 + B/D^{12} \tag{5}$$

Energy, E, has an inverse power law dependence on distance, D, with the $-1/D^6$ term representing the attractive component of the van der Waals force. The absolute value of this term is maximized at a distance D_e where the fluctuations in charge density coincide to result in a potential well. At separations less than D_e, the potential rises rapidly with distance, $1/D^{12}$, as the interaction is repulsive in nature due to electronic overlap and nuclear interaction (Israelachvili, 1992; Cygan, 2001). Force microscopy (or AFM), however, does not record energy values directly, but instead measures force. To compare the Lennard–Jones potential with an AFM data set, we take its derivative, such that graphing the relationship

$$\mathrm{d}E/\mathrm{d}D = F(D) = -6A/D^7 + 12B/D^{13} \tag{6}$$

produces a theoretical force–separation distance curve similar to the one in Fig. 3a. To further facilitate comparison with the theoretical curve, an origin is defined for the force microscopy data set as follows. A force equal to zero can be defined as the average force value within the region of no contact, while the point at which the tip and sample come into (for approach) and out (for retraction) of contact can be defined as the zero point on the x-axis. Determining the point of contact is clear when a distinct attractive or adhesive component (e.g., a jump to contact) is present, but ambiguous when such features are absent. In the latter case, the intersection between the slope of the region of no contact and constant compliance can be used as a guide (Cappella and Dietler, 1999). In a final important step, the x-axis in the force microscopy data set is adjusted to reflect tip sample separation instead of piezo movement, by adding the cantilever deflection values to the piezo movement distances (Ducker *et al.*, 1992; Butt *et al.*, 1995). Here the selection of the sign convention for the forces becomes intuitive. Addition of positive repulsive deflections to the piezo movement results in larger tip-sample separation, while adding negative attractive deflections result in a decrease in the separation. Unlike the Lennard–Jones curve, note that the values in Fig. 3b, left of the point of contact

are essentially meaningless in terms of interaction force because the tip and sample are in direct contact. The end result is a force *versus* tip-sample separation plot with a region of interaction that can be compared to the theoretical curve (see Fig. 3a and b; also see Section V, below).

Two main differences exist between the force microscopy data and the potential: (1) the slope of the attractive component of each curve, and (2) the hysteresis that exists between the approach and retraction forces in the force microscopy plot. With the force microscope, it is not uncommon to record

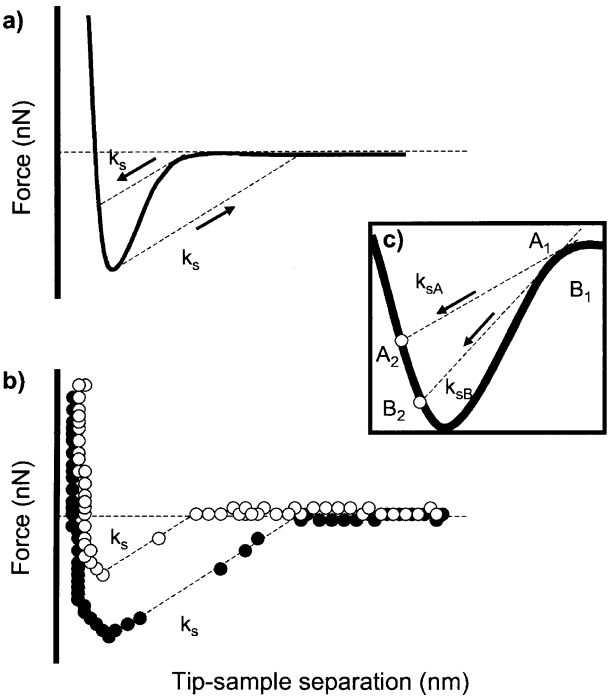

Figure 3 (a) Differentiated Lennard–Jones potential provided as an example interaction to be captured with force microscopy or AFM. During AFM operation the forces associated with the potential are recorded as deflections in the cantilever. If the force gradient (tangent to the solid trace) exceeds the spring constant, k_s, the cantilever becomes mechanically unstable and will jump along a slope equal to k_g (dashed line). (b) Force–tip sample separation curve showing jumps to and from contact along slope $= k_g$. Unlike Figure 2, the *x*-axis represents separation distance between the tip and the sample. Here, both the approach (open circles) and the retraction (closed circles) traces are shown. Note that the hysteresis between the two traces is absent in the Lennard–Jones curve where the solid line represents both approach and retraction forces. Points to the left of zero separation (i.e., lowest most point on the approach or retraction curves) represent movement of the piezo while the tip and sample are in contact. (c) Increasing the spring constant (e.g., using a stiffer cantilever) from k_{sA} to k_{sB} will capture more of the potential (region A_2–B_2), however force resolution is lost and smaller magnitude forces will go undetected.

an attractive force as a characteristic jump to contact on approach. These "jumps" represent mechanical instability in the cantilever due to a force gradient that exceeds its spring constant, k_s. Clearly, interaction information is lost as the cantilever encounters a force gradient (tangent to the theoretical curve) at point A_1 that is greater than its stiffness and consequently jumps to point A_2 along a slope equal to k_{sA} (see Fig. 3c). More of the attractive potential can be sampled with a stiffer cantilever (e.g., k_{sB}), however, force resolution is lost, and the region along the theoretical curve between B_2 and A_1/B_1 remains unsampled. A similar situation may be encountered upon retraction, which, in part, contributes to the hysteresis observed in the force data. Specifically, cantilevers with smaller spring constants generate larger amounts of hysteresis. However, hysteresis between approach and retraction curves is also due to the formation of adhesive bonds once surfaces are in contact. This is common for soft samples such as biological cells (see below). For some investigations excessive hysteresis is undesirable and several techniques have been developed to reduce it thereby recovering the "lost" information (i.e., region A2–B2). These methods employ an opposing force that is external to the system in an attempt to increase the effective stiffness of the cantilever, while retaining force resolution. Electrostatic force (Joyce and Houston, 1991), magnetic feedback (Jarvis *et al.*, 1996; Yamamoto *et al.*, 1997; Jarvis *et al.*, 1998; Ashby *et al.*, 2000) and radiation pressure from a laser (Aoki *et al.*, 1997; Tokunaga *et al.*, 1997) have all been used to supply the steadying force to the cantilever.

B. Hysteresis

Certainly other sources besides the instability of the cantilever contribute to approach–retraction hysteresis. In the theoretical Lennard–Jones relationship given as a potential example, no adhesive reaction between the tip and sample is modeled and the retraction curve retraces the approach curve (Fig. 3a). However, this is not an appropriate model for soft biological cells, which have biopolymers, designed over millions of years of evolutionary selection, for the express purpose of adhesion. When making force microscopy measurements, the tip comes into contact with the surface allowing for reaction and deformation between the two. The bonds and coordinations that result can then be explored and characterized using the associated adhesion forces and approach-retraction hysteresis (Burnham *et al.*, 1990; Cappella *et al.*, 1997). In some systems, the number of bonds that form (and, thus the level of hysteresis) is correlated with the amount of pressure that is applied on the sample by the tip (Weisenhorn *et al.*, 1992). Specifically, increased pressure leads to sample and tip deformation resulting in increased contact area (Israelachvili, 1992; Cappella *et al.*, 1997), and in the case of functionalized tips (e.g., those coated with self-assembling organic monolayers), a possible rearrangement of functional groups terminating the monolayer.

Both phenomena facilitate additional bonding, larger hysteresis and higher adhesion values, as documented by several workers (Weisenhorn *et al*., 1992; Hutter and Bechhoefer, 1993; Toikka *et al*., 1996; Ashby *et al*., 2000). Therefore, the amount of indentation must be carefully documented to facilitate the comparison of adhesion data from one study to another. One way of controlling the amount of indentation using commercially available AFMs is by adjusting the scan start position, setpoint or the trigger settings. Varying these parameters can be especially useful when probing many biological systems, where pressure and/or contact time may be a natural mechanism of inducing adhesion (e.g., see Leckband and Israelachvili, 2001; Lower *et al*., 2001a).

C. Tip Shape

Tip shape is a critical AFM parameter that can dictate the force values and contact geometry between the sample and force probe (Hartmann, 1991; Butt *et al*., 1995). Constraining this value is essential if experimental force traces are going to be compared theoretical models such as "DLVO" (see Section V below). Yet, tip shape can be difficult to determine, in part due to the surface roughness, irregularities and asperities that are associated with traditional silicon or silicon nitride tips (Cappella *et al*., 1997). Moreover, tip shape can change over time as continued use promotes wear (Cappella *et al*., 1997). Solutions to this problem include careful, periodic characterization of the tip with electron microscopy, better constraint of tip geometry by attaching a spherical colloidal probe (Ducker *et al*., 1991; Butt *et al*., 1995), or, as described in more recent work, by attaching a carbon nanotube (Wong *et al*., 1998a; Hafner *et al*., 1999; Cheung *et al*., 2000).

D. Spring Constant Determination

If a quantitative analysis of absolute force values is desired, determination of the spring constant (k_s) is critical and nominal values provided by the manufacturer generally cannot be relied upon (Lower *et al*., 2001b). Many factors affect the spring constant including primary characteristics such as cantilever dimensions, geometry and substrate material; as well as, additional modifications common in force spectroscopy such as gold coating, the addition of organic monolayers, the attachment of colloidal spheres or cells, and even ion adsorption (Sader *et al*., 1995; Craig and Neto, 2001; Cherian and Thundat, 2002). As a result, a large body of literature detailing several methods of directly determining k_s exists. A procedure commonly used because of its simplicity, non-destructive nature, and applicability to common cantilever geometries (e.g., V-shaped, rectangular) is provided by Cleveland *et al*. (1993). This method

derives the spring constant by measuring changes in the cantilever's resonance frequency after small masses (e.g. W microspheres) are loaded onto the end of the tip. The Cleveland method is further optimized when corrected for errors introduced by off-end loading of the mass (Sader *et al*., 1995). More recent methods measure hydrodynamic drag of the cantilever through a fluid of known viscosity to determine k_s for bare rectangular cantilevers (Sader, 1998; Sader *et al*., 1999; Maeda and Senden, 2000). This concept has also been applied to determine k_s for cantilevers activated with a colloidal probe (i.e., a silica or polystyrene microsphere) (Craig and Neto, 2001). In the latter method, it is useful to directly measure k_s for a cantilever with an attached sphere because it accounts for changes in the spring constant due to the shifts in the point of load associated with the position of the colloid sphere and the change in the stiffness associated with the adhesive used for microsphere attachment. Other methods measure k_s using thermal oscillations and the equipartition theorem (Hutter and Bechhoefer, 1993; Butt and Jaschke, 1995), a finite element analysis of the static deflection of a cantilever for which the Young's modulus is known (Sader and White, 1993); unloaded resonant frequency of a cantilever of known mass (which is commonly not the case) (Sader *et al*., 1995), radiation pressure from an acoustic transducer (Degertekin *et al*., 2001); microscopic and macroscopic reference cantilevers of known stiffness (Rabinovich and Yoon, 1994; Torii *et al*., 1996; Jericho, 2002); and the change in resonant frequency due to gold coating (Gibson *et al*., 2001).

E. Artifacts in Force Measurements

Several artifacts can arise during force measurements with the AFM. The inverse path effect represented as an upward, hysteretic shift in the retraction trace in the region of contact arises from nonlinearities of the piezoelectric actuator that positions the sample (or tip) (Cappella *et al*., 1997; Cappella and Dietler, 1999; Heinz and Hoh, 1999). A shift in the contact portion of the retraction trace such that it is parallel with the extension trace reflects friction as the tip plows or slides along the surface (Heinz and Hoh, 1999). A sinusoidal oscillation in the region of no contact may also be present, representing the interference of stray laser light bouncing off the sample and interfering with the laser light reflected off the top of the cantilever (Weisenhorn *et al*., 1992; Cappella *et al*., 1997). This oscillation can be distinguished from other artifacts, such as noise due to mechanical vibrations, because its wavelength should roughly be equal to $\sim \lambda/2n$, where λ is the wavelength of the laser source and n is the index of refraction of the fluid between the tip and sample (Weisenhorn *et al*., 1992; Craig and Neto, 2001). Thermal oscillation in the region of contact can be recognized by deflection fluctuations whose standard deviation is roughly equal to $(k_s k_B T)^{0.5}$; k_s, the spring constant; k_B, Boltzmann's constant and T, temperature (Gergely *et al*., 2001). Operational artifacts may include a large slope that is

present in the region of no contact, common when making measurements in a fluid cell. The origin of this slope is unclear but can often be remedied by eliminating air bubbles in the system or insuring a flat, even orientation of the gasket used to seal the system. Large plateaus at the extremities of both traces often represent a saturation of the detector, requiring an adjustment of the scale of the plot, the deflection limit of the detector or the starting position of the scan.

F. Data Processing and Statistics

With standard AFMs, the one-click ease with which a single force curve is collected allows hundreds of curves to be recorded at a sample point in only a few minutes. Considering the fact that a typical curve can contain 2048 data points, a single experiment can produce an enormous volume of data. Further, the variability between force curves collected at a single location can often be quite high. This raises several questions regarding data processing and interpretation that are often neglected. What is the most efficient way to process these data? What is the minimum number of curves necessary to characterize each sample point or a particular interaction? What level of error and variability is associated with the force measurements? How is force data distributed about its mean? What measurable parameters or features of a force curve are the most important in characterizing the interactions (e.g., adhesion force)? What is the best way to identify trends or correlations in these parameters? Clearly, answering these questions requires statistical techniques, tests and models that determine appropriate, significant average values of force curve parameters and facilitate the identification of meaningful force curve features.

This process begins by collecting summary statistics for each data set, including calculation of means, standard deviations, error values (e.g. confidence limits) and by plotting histograms for multiple parameters derived from the curves, including adhesion force and distance of jump to contact. When comparing parameters from the curves, statistical tests (e.g. ANOVA, *t*-tests; correlative tests) may be performed using a standard statistical and data processing package (e.g., Igo Pro, Wavemetrics, Inc.). Simple regression models may also be employed to determine important variables that contribute to the shape of a force curve. To this end, a routine has been written (Kendall and Hochella, 2003) that rapidly processes force curve data to produce plots of force *versus* piezo movement and force *versus* tip sample separation using the procedures discussed above. Automated parameter determination, statistical calculations, whole force curve averaging, autocorrelation calculations (for identifying quantized force values) and histogram generation are incorporated in this customized routine written using Igor Pro's internal programming environment. The simple parameter extraction module quickly and consistently identifies features and selects the values using basic, objective criteria such as

maxima thresholds in the differentiated force data and tolerance limits for specific changes in slope (see Fig. 4).

G. Advanced Algorithms

These criteria are appropriate when the bond ruptures and snaps to contact are large and/or distinct. However, other more advanced algorithms (Baumgartner *et al*., 2000; Kasas *et al*., 2000; Gergely *et al*., 2001) are required when features are small, numerous, less distinct (e.g., multiple ligand–receptor interactions) and/or have the potential to be masked by vibrational and thermal noise. For example Kasas *et al*. (2000) employ a fuzzy logic algorithm that enables automated discrimination of specific, significant adhesions in a retraction curve that might otherwise be overlooked. The routine assigns a grade to each potential rupture event, ranking it somewhere between non-specific (0) and specific (1). Assignment of the grade relies on *a priori* knowledge of the interaction event morphology, and uses criteria such as the angle between the jump and the background trace, or whether or not the jump is U-shaped or V-shaped. This means that the procedure is operationally defined and first has to be "taught" what the features of interest look like in order to calibrate it to the system/features being studied.

Gergely *et al*. (2001) present an algorithm that identifies ruptures based on a comparison of the minima with neighboring peaks. Selection is controlled by adjusting an appropriate noise level, m, such that the difference between a feature and its nearest neighbors must be greater than $2m$ times the standard deviation of the force values. Additional smoothing of the force curve is also achieved by fitting a second order polynomial to a designated amount, p, of consecutive points. Using this routine, forces measured between human fibrinogen interacting with a silica surface were processed. By monitoring histograms of inter-rupture distances selected with successively more rigorous (higher) m values, the authors were able to detect a significant peak at 20–25 nm, a value that corresponds nicely to the known spacing between two domains in the protein.

H. Relating Bond Chemistry and Energies to Force Measurements

Force microscopy measurements intuitively have the potential to describe energies, $E(D)$, associated with an interaction at a small separation, D, by integrating force over distance, $E(D) = \int F \, \mathrm{d}D$. As discussed above, however, differences in spring constants can produce variable hysteresis and, therefore, can lead to drastically different energy values. Without fine control of the effective spring constant, it is difficult to accurately capture a potential in a quantitative fashion, which is critical for single molecular work. Moreover, if reaction occurs

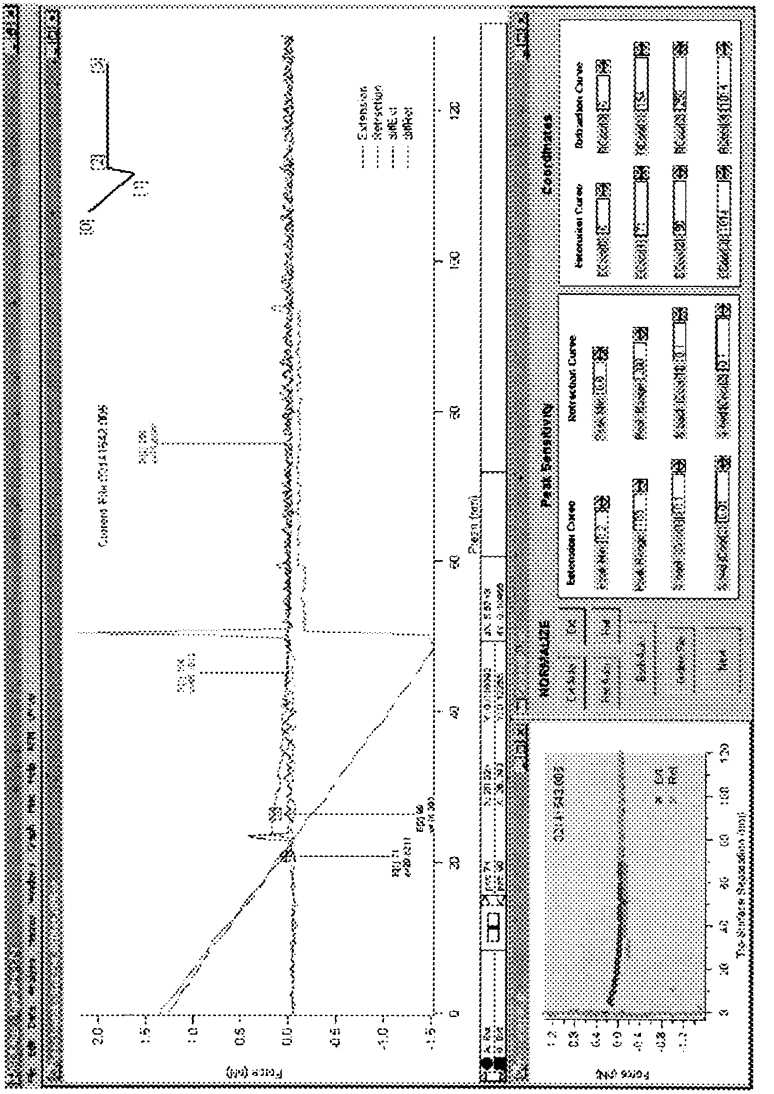

upon contact (and provided single interactions can be identified in the force spectra); simple prediction of bond/interaction energies based on rupture forces is non-trivial. Specifically, it might be postulated that the maximum gradient in the potential, $[\mathrm{d}E/\mathrm{d}D]_{\max}$, is equal to the adhesion or rupture force from the retraction trace; however, in a seminar paper, Evans and Ritchie (1997) showed that such a simple correlation is not valid for single molecule interactions, and more sophisticated theory is required for quantitative comment on the absolute energetics of a bond using force data.

Before continuing, it must be noted that these findings do not preclude valuable quantitative and qualitative comparison of force measurements and bond ruptures to energy parameters. Indeed, early force experiments with various ligand receptors (e.g., biotin, iminobiotin, avidin, streptavidin combinations) revealed a correlation between the rupture forces and enthalpy values associated with each complex (Moy *et al.*, 1994a). This information together with the lack of correlation between the rupture forces and total free energy suggested the unbinding was adiabatic and that any entropic contributions to the system (e.g., solvation forces) occurred outside of the binding pocket, and were not recorded with the AFM. Other studies followed, relating thermodynamic parameters to interaction forces (Chilkoti *et al.*, 1995), as well as many force experiments that employed "elementary" or averaged rupture forces to compare two or more systems in a relative fashion (Florin *et al.*, 1994; Frisbie *et al.*, 1994; Dammer *et al.*, 1996; Noy *et al.*, 1997; Ito *et al.*, 1999; Schmitt *et al.*, 2000; Fiorini *et al.*, 2001; Lower *et al.*, 2001a; Kreller *et al.*, 2002; Kendall and Hochella, 2003;). The true value of these studies is their relative quantitative and qualitative comparisons of force data. These characterize the nature of forces at an interface, demonstrate surface and molecule recognition, and define relative affinity between two molecules or between a molecule and a surface. However, Evans demonstrated that these rupture forces, as absolute values, represent one point in a continuum of bond strengths (Merkel *et al.*, 1999); and that the detachment force recorded with the AFM (and other force measuring techniques) is not a singular fundamental

---

Figure 4 Screen shot of one module (Sensitivity Tweaks) in the force curve processing routine AFM 4.4 written in Igor Pro, 4.04, WaveMetrics, Inc. (Kendall and Hochella, 2003; some of the base code was provided by H. Skulason). It is designed primarily for handling force data produced Digital Instrument's Nanoscope IIIa MultiMode system. The Sensitivity Tweaks module is designed to rapidly review and assess how well the normalizaiton routine automatically registers and normalizes force data to an origin. The normalization procedure includes the identification of a baseline in the region of no contact, calculating the detector sensitivity from the region of constant compliance and detecting when the tip and the sample are in contact. The latter is determined using peaks in the differentiated force wave that are selected based on threshold/sensitivity settings shown in the panel in the lower right. If initial normalization is unsatisfactory, these settings may be optimized and an auto-normalization may be run again; or features can be identified manually.

property of the molecular interaction being probed (Evans and Ritchie, 1997; Evans, 1998; Merkel *et al*., 1999). Instead, apparent bond strength as estimated by rupture force is a function of the loading rate (Evans and Ritchie, 1997).

This relationship represents a refinement of a model proposed by Bell (1978) that predicts an exponential amplification of dissociation kinetics in the presence of an external force (Merkel *et al*., 1999). Dissociation of relatively weak associations can be conceptualized as a particle moving out of a potential well (bond), over single (simple interaction) or multiple (complex interaction) activation barriers representing transition states (Fig. 5). Under a zero force condition the particle will migrate out of the well, through the transition states, and ultimately to complete dissociation on a time scale that is dictated by thermal agitation (k_BT). A constant external force on the bond, however, expedites the thermally mediated kinetics and decreases the lifetime of the bond by lowering the activation barriers in the energy landscape along a projection that is proportional to the amount of force (Fig. 5) (Evans and Ritchie, 1997). Under a dynamic load (e.g. a retracting cantilever) where the force, F, increases over time, t, as loading rate, $R_f = dF/dt = k_s v_c$ (k_s is the spring constant of the system and v_c is the velocity of the cantilever), inner activation barriers are revealed as outer activation barriers are progressively lowered by the accumulating force. This

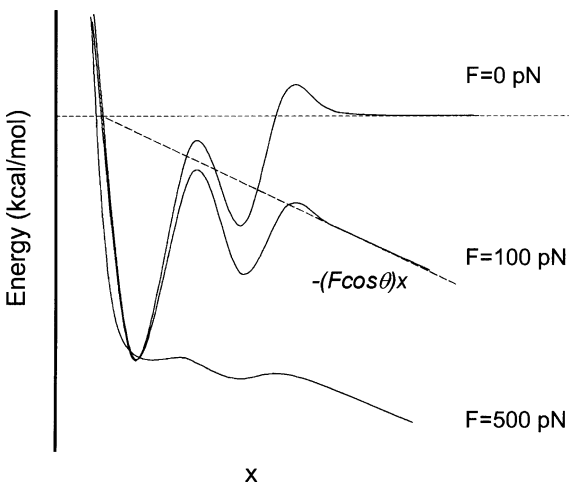

Figure 5 The effect of an external force on the energy landscape of a bond. (Modified from Evans and Ritchie, 1997; Merkel *et al*., 1999). The minimum of the traces represents a bond or potential well found along a reaction coordinate, x. Two activation barriers (local maxima) exist representing transition states that a system must go through during dissociation of the bond. External force, F, is represented as a mechanical potential, $-(F \cos q)x$ oriented at an angle θ to the reaction coordinate. Increasing force lowers outer activation barriers to reveal the inner maxima. Eventually all barriers are lowered allowing free diffusion from the initial minimum/bond (Evans and Ritchie, 1997).

phenomenon leads to an intriguing positive correlation between the rupture force, F_r, and $\log_e(R_f)$, that is best conceptualized in terms of thermally mediated nature of the bond rupture kinetics. At small loading rates, activation barriers are lowered at a rate slow enough for thermal contributions from the medium to be effective in helping the molecule diffuse out of the well and over the barrier before higher forces are reached (Gergely *et al*., 2002). Thus, with an effective thermal contribution, a lower rupture force is recorded at the time of dissociation. Under large loading rates (e.g., those typical of many AFM experiments), activation barriers are lowered fast enough such that dissociation proceeds with minimal thermal contribution, resulting in a higher rupture force (Gergely *et al*., 2002). At ultrafast loading rates on the time scale typical of molecular dynamic (MD) simulations (10^{12} s), the entire bonding potential is compromised quick enough that only frictional drag is recorded as the molecule traverses a completely "stretched" and coarsened energy landscape (Evans and Ritchie, 1997). Here, loading rates commonly exceed the time scale of unencumbered, diffusive passage of a molecule from its bonded state, leaving the complex kinetically trapped as force continues to rise. This was observed during molecular dynamic simulations of the biotin–streptavidin complex (Grubmuller *et al*., 1996). For the biotin system, the time for diffusive passage, t_D (e.g., the lifetime of the bond) is estimated to be 500 ps under a constant force of 280 pN (Evans and Ritchie, 1997). All activation barriers are lowered at this force such that the initial minimum (e.g., the original potential well representing the bond) is exposed allowing direct diffusion out of the well. However, the ultrafast molecular dynamic simulation loading rate (1.3×10^{12} pN s^{-1}) exceeds 280 pN/t_D, therefore, leaving the complex kinetically trapped in the bound state as rupture force rises well above 280 pN (Evans and Ritchie, 1997).

With these observations and extensive theory development, Evans recognized that measurements of rupture forces over a large range of loading rates effectively probes the lifetime of the interaction under different levels of force while mapping out energy barrier position and heights in a technique now known as dynamic force spectroscopy (Evans, 1998). A dynamic force spectra is constructed by plotting the most probable rupture force of a single interaction, F_r, *versus* $\log_e[R_f]$, where R_f values span several orders of magnitude. Regions of constant slope defined as $f_b = k_B T/x_\beta$ represent activation barriers at a distance of x_β from the potential well. Barrier heights E_b can be derived from the intercept of the slopes at zero force defined as (Evans and Ritchie, 1997):

$$log_e(R_f^o) = -E_b/k_B T + log_e(f_b/t_D) \tag{7}$$

where, again t_D is the time of diffusive passage, and thus $1/t_D$ represents an attempt frequency. The attempt frequency is generally not known, but can be estimated from the damping phenomenon (Evans, 1998). Activation barrier positions derived from experimental dynamic force spectra of the biotin–avidin

interaction compared well with barriers predicted by molecular dynamic simulations (Evans and Ritchie, 1997; Izrailev *et al*., 1997), further emphasizing the value of coupling force measurements with computer simulations. However, it must be noted that bridging the gap between the orders of magnitude in the loading rate of experimental systems *versus* loading rates used in computer simulations is not straightforward and extrapolation of calculated rupture forces to experimentally determined forces must be done with caution (Grubmuller *et al*., 1996; Izrailev *et al*., 1997; Wong *et al*., 1999). While this was attempted by Grubmuller (1996), Izrailev (1997) and Evans (1997, 1998) indicate that the real value of molecular dynamic simulations, in this context, is their potential to provide clues as to which structural determinants of the interactions contribute to the activation barriers, thereby providing a qualitative mechanism to account for dynamic force spectra features. For example, Izrailev *et al*. (1997) used a collection of molecular dynamic simulation packages to demonstrate a ground state avidin–biotin complex that was stabilized by hydrogen bonds between the biotin head group and polar amino acids (e.g., Tyr33) within the binding pocket. With the application of an external force, two intermediate states stabilized by H-bonds with amino acids at different positions in and near the pocket (e.g., Ser16 and Arg114) are revealed as the ligand is removed — an observation that was consistent with dynamic force spectroscopy experiments.

Lo *et al*. (2002) also used a variation of the Bell model to explore the relationship between rupture force and ambient temperature in the biotin–avidin system. The experiments were conducted on an AFM with a constant, millisecond time scale loading rate that was slow enough, compared to the nano to picosecond time scale of molecular dynamic simulations, to neglect any frictional energy loss due to viscous drag. The slow loading rates also allowed the key assumption that thermal equilibrium is achieved at any moment during the unbinding process. This validated the use of a Maxwell–Boltzmann energy distribution to describe the thermal energy being supplied to the complex. The end result is a relationship (Lo *et al*., 2002):

$$F_i^2 = 2\Delta E_C k_{\text{bond}} - 2k_B T k_{\text{bond}} log_e\left(\frac{\tau_R}{\tau_D}\right) \tag{8}$$

that can be fitted to an experimental AFM data set of adhesion forces (F_i), to derive bond stiffness (k_{bond}), and critical binding energy (ΔE_C). Both the derived values reflect a summation of the different types of forces that make up the biotin–avidin interaction (e.g., H-bonds, van der Waals and polar interactions). Other variables include thermal energy ($k_B T$), and the ratio of the rupture time (τ_R, determined from the AFM data) and time required for the ligand to diffuse out of the binding pocket (τ_D, estimated independently). Critical binding energy, ΔE_C, may be related to a dissociation energy (D_e) by defining a potential to describe the interaction — in this case a Morse potential was used. Their D_e value based on force measurements, 28.4 kcal mol^{-1}, compared favorably with

the enthalpy change of the dissociation determined by independent means ($\Delta H = 23.4$ kcal/mol) (Swamy, 1995; Lo *et al*., 2002). Moreover, the enthalpy value was combined with bond stiffness in additional calculations to determine a critical displacement magnitude (0.1 nm) that was close to inner barrier position, x_β, value determined with dynamic force spectroscopy ($x_\beta = 0.12$ nm).

Both temperature dependent and load dependent dynamic force spectroscopy rely on force measurements of the interaction of a *single* ligand–receptor pair. This is accomplished by reducing the density of the sites that are present and available for bonding (similar to protocols outlined by Florin *et al*. (1994), Rief *et al*. (1997a, b), Marszalek *et al*. (1998) and Grandbois *et al*. (1999)), such that 1 in 7–10 touches results in attachment (Evans, 1998). Governed by Poisson statistics (Evans and Ipsen, 1991; Williams *et al*., 1996), 90–95% of the attachments are predicted to be single bonds. In addition to the biotin–avidin linkage, Poisson distributions are common in force measurements associated with several other systems (Han *et al*., 1995; Williams *et al*., 1996; Wenzler *et al*., 1997; Lo *et al*., 1999; Stevens *et al*., 1999). The probability, $P(n)$, of an attachment representing n linkages follows a defined, Poisson distribution, making it possible to extract the $n = 1$ case from a large number of rupture force measurements (Lo *et al*., 2002). Feedback mechanisms are also employed to control impingement on the sample thereby insuring each approach and retraction cycle has the same magnitude and history of contact force (Evans, 2001). This is especially important when making measurements with biomolecules secured to monolayers that can easily deform on contact to produce various contact areas and configurations, and ultimately different numbers of attachment (Evans, 2001).

Although successful dynamic force spectroscopy experiments have been carried out on a single force measuring instrument (AFM) with a range of loading rates from 100–5000 pN s^{-1} (Yuan, 2000), due to the exponential relationship between kinetic rates and barrier energies (discussed above), dynamic force spectroscopy is optimized when collecting force measurements over a range of loading rates that are different by orders of magnitude. This can require the use of several force measuring techniques including laser/optical tweezers for slow loading rates 1–10 pN s^{-1}, a biomembrane force probe (BFP) for intermediate rates (10–1000 pN s^{-1}) and AFM for fast loading rates (10^4–10^6 pN s^{-1}) (Evans and Ritchie, 1997).

I. Relevance of Dynamic Force Spectroscopy to Biological–Inorganic Interface

Techniques to extract energy information from force spectroscopy were developed primarily using the biotin–(strept)avidin system (Moy *et al*., 1994a; Evans and Ritchie, 1997) due to its relevance to biological systems, non-covalent nature, high affinity and extensive history of experimentation and study. Since

then, dynamic force spectroscopy has been applied to other systems, primarily non-covalent and biological in nature. These include DNA base pair interactions (Strunz *et al*., 1999), unfolding of muscle protein domains (Rief *et al*., 1997a), antibody–antigen interactions (Schwesinger *et al*., 2000) and lipid anchoring in membranes (Evans and Ludwig, 2000) to name a few. Grandbois *et al*. (1999) also made an attempt at using the dynamic force spectroscopy concept to measure the strength of a single covalent bond. Although they produced values for only one loading rate due to the difficulty of collecting individual covalent interactions (H. Gaub, personal communication). Their calculation of rupture force probabilities based on dynamic force spectroscopy methods allowed them to identify the covalent attachment being terminated as a Si–C bond.

Applying dynamic force spectroscopy concepts to AFM data collected on environmental systems has great potential to provide new insight on the interaction energetics and bond chemistry associated with biogeochemical interfaces. This is, in part, because experimental data collected at the molecular level to describe surface reactions between single biomolecules and mineral surfaces is lacking. Traditionally confined to computer simulation (Cygan, 2001), dynamic force spectroscopy now affords a unique, direct examination of energy landscapes associated with some of the non-covalent mechanisms (e.g., H-bonding) assumed to initiate sorption reactions between minerals and ligands (Holmen and Casey, 1996), the possible ionic or covalent binding of a metal in a mineral surface associated with dissolution (Stumm, 1992), reversible and non-reversible adhesion states of colloids or cells to a surface (Absolom *et al*., 1983; Ryan and Elimelech, 1996; Ryan and Gschwend, 1994), mineral and or metal recognition of a mineral structure by membrane bound proteins (Lower *et al*., 2001a).

Perhaps, the true advantage of using dynamic force spectroscopy is realized when used in a comparative framework, for example, dynamic force spectra of cell or biomolecule–mineral interaction before and after structural and functional changes in either (1) the cell surface (e.g., via altered gene expression due to imposed environmental conditions) or the biomolecule (e.g., via point mutations in proteins, functional group substitutions/inactivation in ligands) or (2) the mineral via metal substitution or by comparing isostructural mineral equivalents or different crystal growth faces. Changes in slopes of the dynamic force spectra resulting from structural modifications can provide clues as to which proteins, functional groups or even crystallographic constraints contribute to surface complex stability or specific activation barriers to binding or detachment. Concomitant correlation of force values with independently determined thermodynamic parameters can also provide insight as to whether a surface attachment or detachment or metal extraction is enthalpy driven or entropically dominated. And as seen above, a common theme when using dynamic force spectroscopy is to supplement and validate characteristics of a particular energy landscape with mechanistic information derived from computer simulations.

The role of these simulations is anticipated to be just as important when applying these techniques to biogeochemical systems.

IV. FORCES AT THE BIOMOLECULE–MINERAL INTERFACE

Organic ligands produced by microorganisms such as low molecular weight organic acids and siderophores have the potential to greatly impact the geochemistry and ecology of soil environments (Stone, 1997; Hersman, 2000). These ligands interact with mineral surfaces to form a critical interface that has implications on biological nutrient/metals acquisition, control of metal toxicity or even ecological competition (Bossier *et al*., 1988; Stone, 1997; Neubauer *et al*., 2000; Brantley *et al*., 2001; Kraemer *et al*., 1999, 2002). Ligands enter into sorption and desorption reactions with minerals that enhance dissolution or surface passivation, mediate contaminant mobility, or alter the charge character of the mineral surface (Barker *et al*., 1997; Stumm, 1992). As a result this interface has been studied extensively with bulk experiments and sorption studies (e.g., Kummert and Stumm, 1980; Ludwig *et al*., 1995; Yao and Yeh, 1996), and with surface sensitive techniques such as XPS (Kalinowski *et al*., 2000), and Fourier Transform Infrared (FTIR) Spectroscopy (Hansen *et al*., 1995; Holmen *et al*., 1997). Key to sorption and desorption reactions between ligands and minerals, however, are the forces that bring the ligand into and out of contact with the surface. Such forces are dependent on the charge character, structure and reactivity of the ligand, the mineral surface and the intervening solution. Characterization of these forces using force microscopy holds great potential to complement information from the existing methodologies listed above in addition to providing new insight on how ligands interact and coordinate with mineral bound metals.

In pioneering work, activation of an AFM tip with a specified chemistry was carried out to examine the biotin–avidin interaction (Florin *et al*., 1994; Lee *et al*., 1994b). Florin *et al*. (1994) sorbed biotin (an organic ligand) to an AFM tip, and probed a surface coated with the protein receptor avidin. Force measurements of this high affinity ligand–receptor system showed a positive correlation between the elementary quantized adhesion forces detected with an autocorrelation analysis and the thermodynamic binding affinities. Specifically, biotin adhesion to the avidin substrate measured 160 pN, while iminobiotin, which contains a nitrogen substitution in place of an oxygen and has a lower binding affinity, exhibited adhesions closer to 85 pN.

Several force spectroscopy studies of the biotin system followed (Moy *et al*., 1994a, b; Chilkoti *et al*., 1995; Wong *et al*., 1999; Lo *et al*., 2002), along with other force investigations of biomolecules, including examination of: interactions

between antibodies and antigens (Dammer *et al*., 1996; Hinterdorfer *et al*., 1996; Schwesinger *et al*., 2000); enzyme activity (Fiorini *et al*., 2001); proteoglycans (Dammer *et al*., 1995); observations on the stretching of polysaccharides (Rief *et al*., 1997b; Marszalek *et al*., 1998) and muscle proteins (Rief *et al*., 1997a); and the hybridization of oligonucleotides (Lee *et al*., 1994a; Mazzola *et al*., 1999). Simple functional groups have also been covalently attached to AFM tips in order to explore more fundamental interactions, such as the forces between methyl, carboxyl or methyl–carboxyl pairs (Frisbie *et al*., 1994; Noy *et al*., 1997). Specifically, this technique, termed chemical force microscopy (CFM), was used to identify the nature of the interacting force (H bond, van der Waals, electrostatic), characterize surface energies and charge distributions, and generate force maps that showed the spatial arrangement of simple functional groups or hydrophobic regions on a monolayer or surface, sometimes with nanometer resolution (Noy *et al*., 1997).

Collectively, these studies provide a foundation, which allows the application of force spectroscopy to additional, more complex, natural systems, such as the ligand/biomolecule–mineral interface that is characteristic of soil environments. Indeed the same forces (e.g., H-bonding, hydrophobic/hydrophilic forces, the van der Waals force, steric forces, non-specific and specific interactions) that allow molecular recognition between biomolecules are also present in ligand mineral interaction (Israelachvili, 1992; Stumm, 1992). However, to our knowledge, only two studies, one of which is summarized below, have probed ligand interaction with a mineral surface using force microscopy (Kendall and Hochella, 2003; Kreller *et al*., 2002). A discussion of this burgeoning application begins with a description of protocols enabling linkage of a ligand to an AFM tip.

A. Ligand Linkage Schemes

Devising a suitable linkage scheme to attach the ligand of interest to the AFM probe can present a significant challenge. Each scheme should be appropriately tailored to the relevant experimental goal; however, the following summarizes general considerations. Successful linkage will provide a strong (e.g., covalent or stronger than the interaction of interest), reproducible bond between the ligand and the tip while avoiding non-specific interactions associated with the cantilever material, tip or linker molecule (Wagner, 1998; Fiorini *et al*., 2001).

Simple ligands such as carboxylate and phosphate groups are commonly linked as terminations of alkylthiol monolayers that coat the tip (Noy *et al*., 1997; Kreller *et al*., 2002). The ampiphilic molecules of the monolayer not only provides an anchor for the ligand but also serves as a spacer, providing separation between the ligand and the tip material thereby reducing non-specific interactions. Larger ligands and proteins that contain either a free amino or carboxyl group may be attached using an active ester technique commonly used

to couple two proteins (Cheung *et al*., 2000; Fiorini *et al*., 2001; Hinterdorfer *et al*., 2002; Kendall and Hochella, 2003). In the presence of a carboxyl group, 1-Ethyl-3-(3-Dimethylaminopropyl) carbodiimide (EDC) together with *N*-hydroyxsuccinimide (NHS) will form a stable, hydrolysis resistant, active succinimidyl ester that readily forms a peptide bond with an available amino group (Grabarek and Gergely, 1990). Note that the position of the amino and carboxyl groups can vary with one being supplied as a self-assembling monolayer (SAM) terminal group on the tip and the other contributed by the molecule to be attached, or vice versa. Other linkage protocols employ polyethylene glycol (PEG) as a cross-linking spacer that is terminated with various functional groups such as pyridildithiopropionate (PDP). PDP coordinates with thiol groups and nitrilo-triacetic acid (NTA) which, in combination with various divalent metals, binds to consecutive histidine residues (Kienberger *et al*., 2000; Schmitt *et al*., 2000; Hinterdorfer *et al*., 2002). One advantage in using PEG-NTA-Me^{2+}-His linkage system is that selection of the divalent metal (Cu^{2+}, Co^{2+}, Ni^{2+}) permits control of the binding force, and, to a certain extent, the probability of the linkage. In addition, the NTA-Me^{2+}-His bond is easily reversible, such that it can be terminated with the use of EDTA, and then regenerated with the reintroduction of the free metal (Schmitt *et al*., 2000). Other workers propose attaching ligands or molecules via carbon nanotubes that extend from the AFM tip (Wong *et al*., 1998a, b, Hafner *et al*., 2001). This provides ideal spacing between the molecule and the tip, but more importantly, drastically increases the resolution of the force spectroscopy (and imaging) due to the nanotube's extremely small radius of curvature compared to a traditional Si_3N_4 tip. Because nanotubes can only be functionalized at the end termination of the carbon lattice this also places an important constraint on the orientation and localization of the molecules being linked. As a result, the probability of capturing a single molecule interaction is increased, especially when working with lower molecular weight molecules.

It is important that the linkage must not directly interfere with the activity of the ligand (Fiorini *et al*., 2001), and thus, electron donor functional groups should be protected during the linkage reaction. Kendall and Hochella (2003) accomplished this by inserting a metal (Al^{3+}) into the ligand (azotobactin) structure to occupy and protect the chelating groups, while carrying out the linkage reaction. Once attached to the tip, the azotobactin was reactivated by removing the Al with high concentrations of a competing ligand (EDTA), a process that was monitored in a test solution with UV–vis spectroscopy (Fig. 6).

Unfortunately, inherent to fixing a molecule to a surface is a reduction in the degree of freedom afforded to the molecule's conformation. This can result in an alteration or loss of chelation or ligand activity and should be considered. To this end, control activations are often run in parallel to tip activations, where monolayers, linker molecules and the biomolecule of interest are reacted with a flat, Si_3N_4 or SiOH substrate (Fiorini *et al*., 2001; Hinterdorfer *et al*., 2002). Similar in composition to the tip, the flat test substrates serve as a proxy for

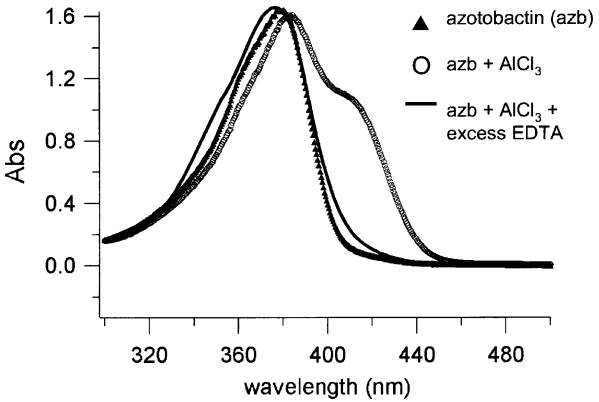

Figure 6 UV–vis spectra showing the transition of Al into and out of the azotobactin (Azb) structure; corrected for dilution. Upon the addition of Al to the system a characteristic shoulder appears in the spectra. This shoulder could be eliminated with high concentrations of EDTA. A similar process was employed to protect and then regenerate the azotobactin chelating groups during linkage of the siderophore to a hydrazide terminated AFM tip (see Kendall and Hochella, 2003).

tip that are readily probed with AFM imaging, fluorescence and confocal microscopy, surface plasmon resonance (SPR) and various enzyme and ligand assays in an effort to assess the success of the linkage reaction; estimate coverage, density and footprint area of the monolayer-biomolecule construct; and evaluate activity retention in the immobilized biomolecule (Fiorini *et al.*, 2001).

B. Siderophores and Oxide Surfaces

Kendall and Hochella (2003) collected force signatures between a ligand (siderophore) and two mineral bound metals (Fe(III) and Al(III)) in an attempt to examine the mechanism of siderophore-mediated dissolution of oxide surfaces. Siderophores are ligands produced by microorganisms to assimilate the essential nutrient ferric iron, in spite of its extreme insolubility in near surface, circumneutral environments. The aqueous chemistry of siderophores has long been studied (Winkelmann, 1991), and it is recognized that their effectiveness in acquiring iron, can, in part, be attributed to a thermodynamic binding affinity for Fe(III) (aq) that has a magnitude above that for other metals, including Al(III). Only recently, however, it was recognized that, in addition to the formation of stable, aqueous iron complexes, siderophores can release iron from minerals (Seaman *et al.*, 1992; Watteau and Berthelin, 1994; Hersman *et al.*, 1995; Holmen and Casey, 1996; Liermann *et al.*, 2000; Maurice *et al.*, 2000). The mechanism of this release, however, is not clearly defined.

Force microscopy of the pyoverdin type siderophore azotobactin interacting with iron and aluminum oxide surfaces showed a unique relationship between

ligand–metal affinity and adhesion forces (Kendall and Hochella, 2003). Average adhesion forces between azotobactin and goethite (α-FeOOH) at pH 7 were 2–3 times the value between azotobactin and goethite's isostructural Al-equivalent, diaspore (α-AlOOH) (Fig. 7a). A similar force relationship was also observed between the trihydroxamate siderophore deferoxamine (DFO) and each oxide surface (Fig. 7b). Control experiments where each mineral surface was probed with a SAM coated tip lacking the azotobactin molecule produced force signatures that were almost identical, indicating the distinction in the force signature between diaspore and goethite could be attributed to the presence of the azotobactin on the tip.

Force measurements collected under various solution conditions (e.g., pH, ionic strength and soluble iron concentrations) and at different sample locations on the mineral extended the characterization of the ligand–mineral interaction and helped identify the source of discrepancy in adhesion values associated with each oxide. As a first guess, it could be hypothesized that the forces of interaction

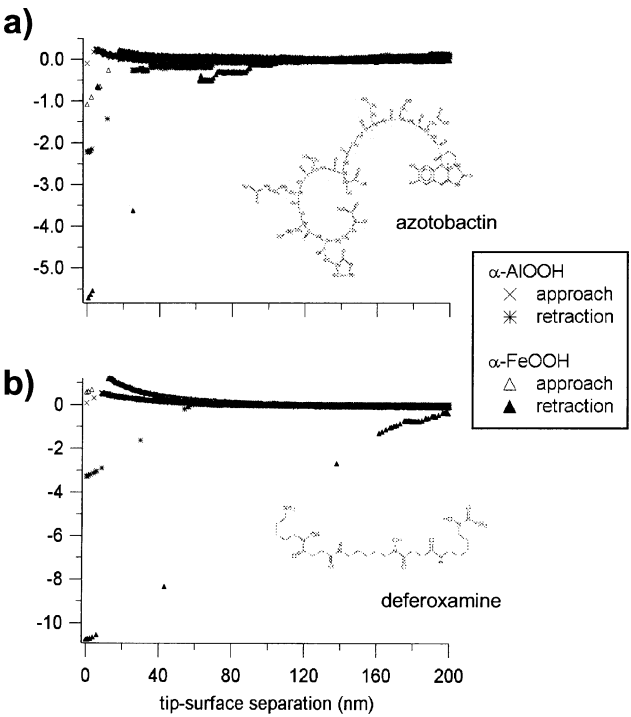

Figure 7 Force spectra showing the interaction of two siderophores (a) azotobactin and (b) deferoxamine (DFO) with goethite (FeOOH) and diaspore (AlOOH) surfaces. Note the large increase in the adhesion force between each siderophore and goethite and versus the adhesion value for diaspore.

are dominated by an electrostatic component; and that the difference in the adhesion values between diaspore and goethite, simply reflects variation in the charge character of each mineral. Although point-of-zero-charge (pzc) literature values for goethite (pzc 7–9) and diaspore (pzc 7–8) are similar, suggesting both should be neutral or slightly positively charged (Cornell and Schwertmann, 1996; Kosmulski, 2001), it is possible that our model system deviates from pristine charge conditions, such that the goethite is positive and the diaspore is slightly negative. With a net negative charge predicted for azotobactin at pH 7 (pK_a hydroxycarboxylate = 4–5; Telford and Raymond, 1996), this could result in a larger adhesion force for goethite presumably due to a stronger electrostatic interaction. Measurements at lower pH and different sample locations, however, suggest otherwise. At pH 3.5, far from the pzc value of each mineral, and where the azotobactin is anticipated to be neutral, the same 2–3-fold increase in adhesion values is observed. Moreover, the azotobactin-goethite/azotobactin-diaspore force relationship remained intact when comparing adhesion distributions representative of different sample locations on each mineral surface, where anomalous charge distributions and changes in microtopography are expected. Overall, similar to observations made with the biotin ligand system (Moy *et al*., 1994a; Chilkoti *et al*., 1995; Izrailev *et al*., 1997), adhesion values upon retraction appear to be relatively independent of protonation equilibria, and may reflect a specific interaction between the siderophore oxygens and the metal contained in each mineral. The discrepancy in adhesion for goethite *versus* diaspore can then be explained by differences in the electronic character of each metal (e.g., Fe(III) *versus* Al(III)), where the more electronegative ferric iron will behave as a harder acid with a higher affinity for the oxygens. In additional experiments with goethite only, this surface affinity was readily disrupted with the addition of soluble iron (Fig. 8). Here, increased [$FeCl_3(6H_2O$] (pH 3.5) led to a saturation of the ligand as the soluble iron out competed the mineral iron for the siderophore oxygens, resulting in lowered adhesion values.

This does not discount an electrostatic component to the azotobactin–oxide interaction. Indeed, decrease in the jump to contact distance with increasing ionic strength thought to reflect a collapse in the double-layer associated with the mineral surface (Noy *et al*., 1997; Lower *et al*., 2000), confirms the effect of charge, especially upon approach. Instead, force evidence suggests a balance between electrostatics dominating the approach and more specific interactions directing surface adhesion; a scheme that is embodied in the following observation — goethite force signatures at pH 7 often show a long range, electrostatic repulsion on approach that was equal to or significantly lower in the diaspore signatures; yet, the goethite adhesion force averaged 3.81 nN compared to 1.38 nN for diaspore.

Force data also provided information on which azotobactin functional groups might be important in the interaction. Distinctive plateaus were commonly observed after retracting the tip ~6–7 nm from the surface (Fig. 9). These features

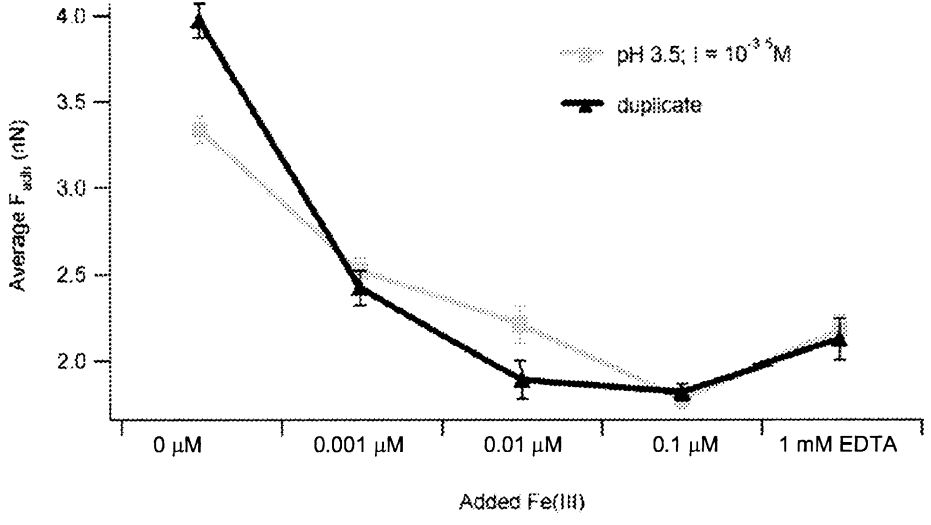

Figure 8 Plot showing decrease in azotobactin–geothite adhesion forces with increasing concentrations of added soluble iron ($FeCl_3$ $6H_2O$). Measurements were collected at pH 3.5 to minimize the precipitation of solid iron phases upon the addition of the iron chloride. Taken from Kendall and Hochella (2003).

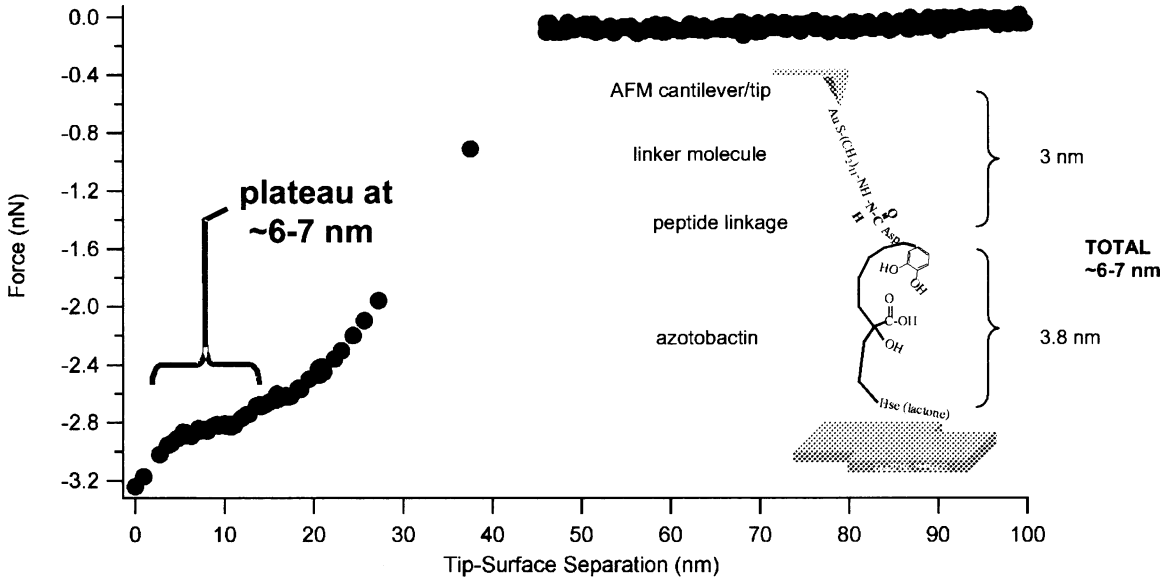

Figure 9 Plateau feature common in many retraction curves while probing oxide surfaces with an azotobactin activated AFM. It is suggested that this feature may represents the extension of the azotobactin and linker molecule during separation from the mineral surface as shown in the inset (not to scale). Also shown in the inset is the geometry of the linkage of the siderophore to the tip. Modified from Kendall and Hochella (2003).

are thought to represent the energy absorption associated with the combined extension and stretching of azotobactin's polypeptide chain and the molecule used to link the ligand to the tip. Using an approximation of 0.38 nm amino acid, a quick calculation shows that azotobactin's fully outstretched length of ~3.8 nm, together with an additional 3 nm from the linker molecule gives a value that is close to the 6–7 nm observed in the force signatures. This distance, then, requires that azotobactin's terminal homoserine group serves as an anchor to the surface, providing a strong, persistent link in the interaction. This coincides with other reports that, in aqueous systems, the adjacent hydroxamate group initiates chelation (Telford and Raymond, 1996; Albrecht-Gary and Crumbliss, 1998). Additionally, considering its terminal position on the molecule, it is feasible that the homoserine group is a dominant component during surface interaction.

Finally, these force microscopy results give cause to reassess the role of large ligands, such as azotobactin, in dissolving minerals. Instead of serving as an Fe shuttle between smaller ligands that interact with the surface and the cell, the force evidence demonstrating azotobactin's strong surface affinity presents a distinct possibility of the relatively large molecule entering into a strong, stable complex with the mineral. As seen above, the force data also allow comment on the nature of the association with the surface. Steric constraints imposed by ligand size, structure and conformation, together with the limited access to an iron atom contained on a mineral surface, would certainly preclude the hexadentate coordination characteristic of the siderophore-aqueous complex (Holmen and Casey, 1996; Hersman, 2000; Cocozza *et al*., 2002). Instead, plateau features in the retraction curves suggest a strong coordination formed by a single oxygen pair that terminates the azotobactin molecule as one possibility. Recent, ongoing MD simulations, in collaboration with U. Becker (University of Michigan), confirm this possibility, as well as the extended dimensions of the azotobactin-linker construct. Interestingly enough, however, simulations reveal that the spacing between the two, chelating hydroxamate oxygens is sufficient to allow individual coordination with neighboring irons in the goethite structure (Fig. 10). Siderophore–oxide interaction continues to be examined with molecular dynamic simulation as well as dynamic force spectroscopy.

V. FORCES AT THE BACTERIUM–MINERAL INTERFACE

A. Force Microscopy Technique Using Whole Cells

The fundamental forces between a bacterium and mineral surface are central to understanding the intricacies of interfacial phenomena such as bacterial

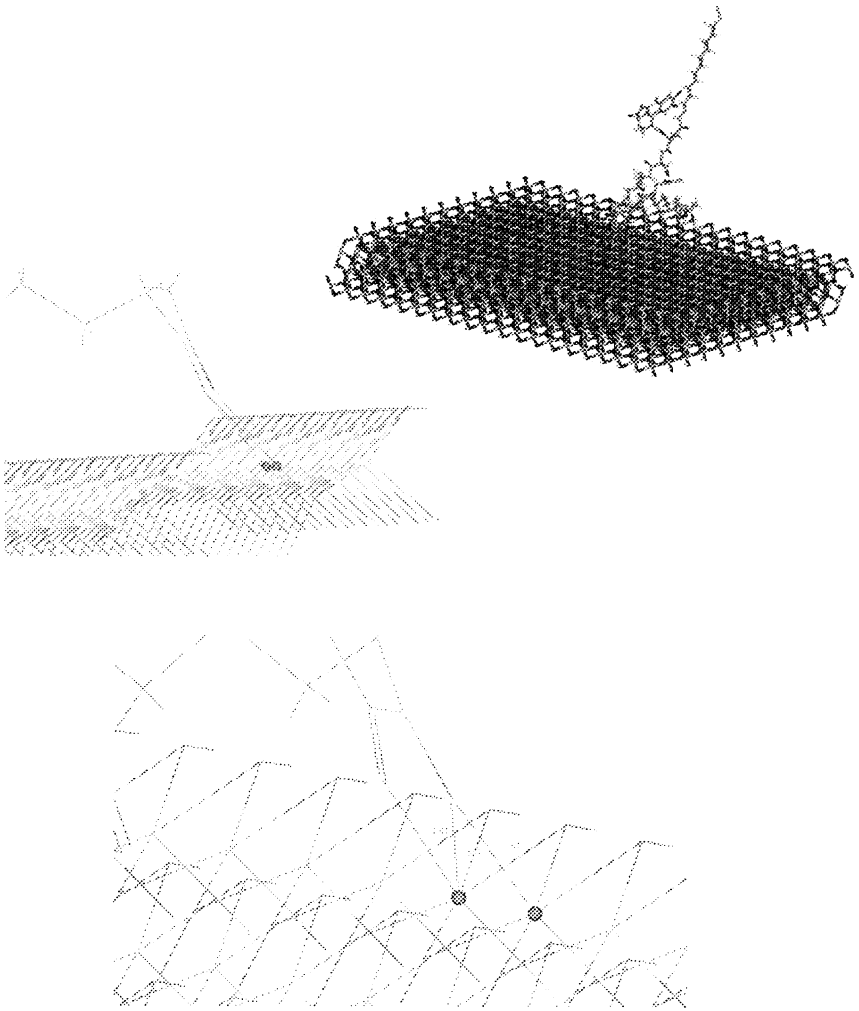

Figure 10 Molecular model of azotobactin (with linker molecule) interacting with a goethite surface. Simulations were completed using Cerius2, Accelrys, Inc. Arrows point to terminal hydroxamate group oxygens interacting and coordinating with irons (balls) in the lattice. Note the spacing of the siderophore oxygens allow for "bonds" (i.e., Fe–O distances $<$2.1 Angstroms) with neighboring irons. With this coordination, the cross-distance between a siderophore oxygen and an iron diagonally across is over 3 Angstroms.

adhesion to minerals and dispersal in the environment (van Loosdrecht *et al*., 1989; Fletcher, 1996), mineral growth and dissolution (Myers and Nealson, 1988; Hiebert and Bennett, 1992; Schultze-Lam *et al*., 1992; Roden and Zachara, 1996; Fortin *et al*., 1997), biofilm formation (Lawrence *et al*., 1991; Davies *et al*., 1998),

and bacterial affinity for or recognition of specific mineral surfaces (Ohmura *et al*., 1993; Fleminger and Shabtai, 1995; Bhosle *et al*., 1998; Dziurla *et al*., 1998; Edwards *et al*., 1998). A myriad of physicochemical interactions occur at biological–mineral interfaces in nature, due to (1) the mosaic of spatially discrete macromolecular cell wall structures on bacteria, (2) the dynamic nature of these structures, and (3) the diversity of mineral surface functionality, topography, and crystallography (Lower *et al*., 2000). As discussed above in section II, these interactions are expected to be governed by the cumulative effects of intermolecular forces (Israelachvili and McGuiggan, 1988; Israelachvili, 1992; Kendall, 1994; Butt *et al*., 1995; Fletcher, 1996; Gay and Leibler, 1999). However, acquiring even an elementary appreciation of these forces presents a daunting challenge, primarily due to the minute scale at which these interfaces must be probed, and the difficulty in developing a technique that preserves the natural intricacies of the bacterial surface (Lower *et al*., 2000).

Measurement of fundamental forces between whole bacterial cells and inorganic phases can be conducted in one of two ways with force microscopy. The first involves "fixing" cells to a solid substrate (e.g., a glass slide) and probing these cells with a force-sensing cantilever. The simplest setup makes use of the sharp tip that is integrated into most force microscopy cantilevers (see above). In many instances, however, this is not ideal because these tips are not well constrained with respect to their geometry and/or area of contact. As shown in section II, this greatly influences force measurements thereby making it difficult to compare measured data to theoretical force models, and impedes the comparison of data collected with different tips. To overcome the limitations imposed by using a sharp tip, Ducker *et al*. (1991) devised a simple yet ingenious solution. They created a "colloidal tip" by attaching a glass bead to the end of a force-sensing cantilever. This bead was then used to probe a flat silicon surface (Ducker *et al*., 1991, 1992), although such a "colloidal tip" could also be used to probe microbial cells on a glass surface. A number of companies, such as Duke Scientific Corporation, Polysciences Incorporated, and Bangs Laboratories Incorporated, sell spheres ranging in size from nanometers to micrometers. A major drawback to this scenario, however, is that it limits the inorganic phases that can be utilized to those materials commonly used to make tips (e.g., silicon and silicon nitride) or beads (e.g., plastic and glass). With the exception of silica (e.g., glass beads), minerals or other inorganic phases cannot be attached to a force-sensing cantilever. Therefore, interactions between bacteria and minerals much employ another technique. That is, the cells must be linked to the force-sensing cantilever, which is then used to probe a particular face on a mineral crystal or other surface.

The first cell to be linked to a force-sensing cantilever was a large mammalian cell (Antonik *et al*., 1997). This cell was not actually "attached", rather it was induced to grow on the cantilever. The researchers conducting this experiment were not interested in measuring forces, which was fortunate because cells grew

on both the top and bottom surfaces of the cantilever. Hence, the cell growth would have affected not only the spring constant of the lever, but it would also alter the optical lever detection system. Nonetheless, this opened the door to a number of other protocols of linking cells to a force microscope cantilever.

It is a difficult challenge to link microbial cells on the order of 1 μm to the end of a cantilever. Early attempts relied on the attachment of cells that had been chemically fixed or treated with harsh chemicals (e.g., gluteraldehyde) (Razatos *et al*., 1998a, b). While these investigations produced some very intriguing force measurements, this type of linkage protocol is often undesirable because the cells are killed in the process. Further, chemicals such as gluteraldehyde are known to denature proteins and other macromolecules. Another method was developed that allowed the force-sensing cantilever to support bacterial cells in a living, native, fully functional state — thereby creating "biologically active force probes" (Lower *et al*., 2000, 2001b). A polycationic linker molecule (e.g., aminopropyl-triethoxysilane or polylysine) can be used to link living bacteria to a small glass bead that is then attached to the cantilever, or the bacteria can be linked directly onto the cantilever itself (Lower *et al*., 2001b). Polycationic linkers work well because many bacteria are negatively charged over a wide range of pH conditions. Hydrophobic molecules (e.g., octadecyltrichlorosilane) are also attractive linkers because many microorganisms have hydrophobic surfaces. Techniques similar to affinity chromatography (e.g., see Pleuddemann, 1991; Egger *et al*., 1992; Rezania *et al*., 1999) may be employed to design tailor-made linker molecules (e.g., ligand–receptor or antibody–antigen) that work on virtually any bacterial species. The use of polycationic linkers, or similar molecules, preserves the natural conformation, structure, and function of the macromolecules on the microbial surface. When live cells are used (i.e., a biologically active force probe), force measurements may be collected under different physiological or environmental conditions in real time (Lower *et al*., 2000, 2001a, b). Finally, for larger microbial cells such as yeast or fungal cells, the "colloidal tip" technique (see above) can be used to glue a single cell to the end of a cantilever (Bowen *et al*., 1998b).

Using these techniques, a number of groups have used force microscopy to measure intermolecular forces at the bacterium–mineral interface (Ong *et al*., 1999; Bowen *et al*., 1998a; Razatos *et al*., 1998a, b; Bowen *et al*., 2000a, b; Camesano and Logan, 2000; Lower *et al*., 2000, 2001a, b). In our laboratories, we have used biological force microscopy (Lower *et al*., 2000) to measure intermolecular forces between living bacteria (e.g., *E. coli, Burkholderia cepecia,* and *S. oneidensis)* and inorganic phases (e.g., muscovite, goethite, diaspore, graphite, and glass) in solutions of varying ionic strength, pH, and oxygen concentration (Lower *et al*., 2000, 2001a, b). Below we will examine the force–distance relationships at the *E. coli*–muscovite and *S. oneidensis*–goethite interfaces. We will concentrate on the forces measured upon approach of a bacterium towards a mineral in the case of the former. For the latter system

(i.e., *S. oneidensis*–goethite), we will explore forces measured as the two surfaces are pulled apart or retracted from one another.

B. Forces between *Escherichia coli* and Muscovite

Figure 11 shows the interaction between *E. coli* and the (001) surface of muscovite as the sodium chloride (NaCl) solution was exchanged five times between low ($\sim 10^{-5}$ M) and high ($\sim 10^{-1}$ M) ionic strength. While both approach and retraction forces were measured, shown in Fig. 11 are only the forces detected upon approach of the mineral towards living cells on a biologically active force probe. At low ionic strength, repulsive (positive sign) forces were detected at a separation of approximately 100 run. This repulsive interaction increased exponentially (see below) to a maximum value of ~30–35 nN at contact. At high ionic strength, the magnitude of repulsion was significantly less as was the range of separation over which force interactions took place. The two surfaces did not "feel" one another until they were within 15–20 nm of separation. As with the measurements at low ionic strength, an exponential force appears to dominate at high ionic strength. It is important to note that these data shown in Fig. 11 span the entire range of measurements for literally hundreds of force–distance curves taken as a solution was exchanged

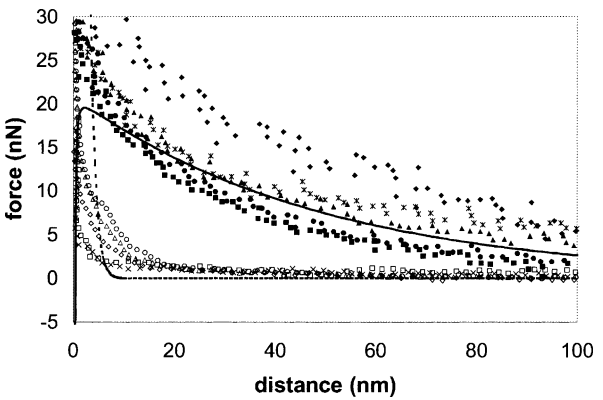

Figure 11 Force–distance relationship between the basal plane surface of muscovite and *E. coli* in solutions of high (open symbols across lower portion of figure) or low (closed symbols across upper portion of figure) ionic strength. Shown for each solution condition are five data curves that span the entire range of measurements for literally hundreds of force-distance curves. The lines correspond to the DLVO model prediction at high (dotted) or low (solid) ionic strength. Repulsive forces have a positive sign; whereas attractive forces have a negative sign. Only those forces measured upon approach of the mineral towards the bacteria are shown. See text for discussion.

several times between high and low ionic strength. Hence, the measurements are reproducible.

Results can be interpreted with the so-called DLVO theory (Derjaguin and Landau, 1941; Verwey and Overbeek, 1948). This theory describes forces (F) as a function of the distance (D) (e.g., between a bacterium, treated as a sphere and a mineral, treated as a flat plane) as the sum of the electrostatic and van der Waals forces (Ducker *et al.*, 1991; Israelachvili, 1992; Butt *et al.*, 1995; Muller and Engel, 1997):

$$F_{DLVO}(D) = F_{electrostatic}(D) - F_{\mathrm{vdw}}(D) = \frac{4\pi\sigma_{bacteria}\sigma_{mineral}R}{\varepsilon\varepsilon_0\kappa}e^{-\kappa D} - \frac{H_{\mathrm{a}}R}{6D^2}$$

where σ is the surface charge density (C m^{-2}), R is the radius of a cell (or in this case the radius of the bacteria coated bead attached to the cantilever), ε is the dielectric constant of water (78.54 at 298 K), ε_0 is the permittivity of free space (8.854×10^{-12} C^2 J^{-1} m^{-1}), κ is the inverse Debye length (Debye length $\sim$1 nm at 10^{-1} M and $\sim$100 nm at 10^{-5} M; see above), and H_{a} is the Hamaker constant. For the model results plotted in Fig. 11, Hamaker's constant was 10^{-21} J (Vigeant *et al.*, 2002); surface charge density of the bacterium was estimated using Eq. (3) as -0.001 or -0.04 C m^{-2} at low or high IS, respectively (surface potential measurements were taken from Camesano and Logan (2000), Ong *et al.* (1999) and Vigeant *et al.* (2002), and the surface charge density of the mineral was estimated using Eq. (3) as -0.004 or -0.2 C m^{-2} at low or high ionic strength, respectively (surface potential measurements were taken from Ducker *et al.* (1992) and Ong *et al.* (1999)).

Figure 11 compares the measured forces with those predicted by DLVO theory. Ionic strength (approx. 10^{-1} *versus* 10^{-5} M) appears to have a strong effect on the interactions between *E. coli* and muscovite. This is because higher salt concentrations cause the electrostatic double-layer to become thinner (i.e., surfaces cannot "feel" one another until they get very close). Further, the increased concentration of counter ions at high ionic strength effectively screens the negative charges on both surfaces, thereby resulting in smaller magnitude forces of repulsion. These particular measurements are fairly consistent with DLVO theory. However, there are some important discrepancies. For example, at low ionic strength the attractive van der Waals force is expected to dominate the interaction at separations less than 5 nm. However, measurements reveal that *E. coli* and muscovite do not exhibit attraction even at the closest approach. Indeed, adhesion forces were not detected when *E. coli* and muscovite were forced together and subsequently pulled apart at low ionic strength (Lower *et al.*, 2000). This suggests that electrostatic and/or other repulsive forces (e.g., solvation interactions) dominate this particular interaction.

Many other force measurements conducted in our laboratories, suggest that electrostatic and van der Waals forces are not the only intermolecular forces at the bacterium–mineral interface (S. Lower, unpublished results). Others have

attempted to invoke extended-DLVO models to explain deviations from purely van der Waals and electrostatic forces and fit model predictions to measurements (see e.g., Ong *et al*., 1999; Camesano and Logan, 2000). While these investigations may be valid, one needs to remember that force models are sensitive to the geometric shapes of interacting particles as well as the roughness of surfaces and contact area (Israelachvili, 1992) all of which are difficult to rigorously define or control for minerals and cells with biopolymers. Further, DLVO was developed to describe the phenomena between inanimate particles rather than living cells that have exquisite control over the expression of surface macromolecules. Seemingly simple concepts such as "contact" become difficult to define for cells having polymers of varying length, which extend for some distance beyond the cell wall. Further, living cells and/or surfaces with polymers are expected to show a time dependent adhesion (measured by Lower *et al*., 2001a) as biopolymers diffuse into the cell wall and reorient with respect to another surface (Beveridge, 1999; Leckband and Israelachvili, 2001). The true value may not be in whether a model perfectly fits data, but the most definite answer comes when the measurements contradict the theory, thereby disproving a particular construct and suggesting that other forces are responsible for a particular bacteria–mineral interaction. As stated by Oreskes *et al*. (1994) scientific investigations are at their best when one combines experimental measurements and model predictions to challenge existing formulations. Hence, there is a great need to test such models by comparing theories to precise force measurements using "model" microorganisms and minerals. Only then will we be able to understand how *all* of the various intermolecular forces (e.g., electrostatic, van der Waals, hydration, hydrophobic, and steric interactions) govern interactions at the bacterium–mineral interface.

C. Forces between *Shewanella oneidensis* and Goethite or Diaspore

The forces required to pull the mineral and bacteria apart (i.e., retraction data) are not shown in Fig. 11. In fact, a very strong adhesion force was detected between *E. coli* and muscovite, but only at high ionic strength (Lower *et al*., 2000). Aside from being a notable example of a situation that DLVO theory often cannot explain, retraction data provide an immense amount of information about the adhesive strength and structural properties of specific biopolymers on a cell's surface. Recently, we interpreted these retraction data for studies of bacterial adhesion and electron transfer reactions between *S. oneidensis* (a dissimilatory-iron-reducing-bacteria) and the minerals goethite (FeOOH) or diaspore (AlOOH) under aerobic and anaerobic solution conditions (Lower *et al*., 2001a; Lower *et al*., 2002). *S. oneidensis* is capable of using either oxygen or ferric iron in the crystal structure of iron oxyhydroxides as a terminal electron

acceptor (Nealson and Saffarini, 1994). We used force microscopy to determine whether a microorganism could discriminate between two very similar minerals (diaspore and goethite) under anaerobic conditions, when electron transfer is expected to occur between *S. oneidensis* and iron containing minerals.

A mineral crystal, mounted on a piezoelectric scanner, approached live bacteria on a biologically active force probe at a rate that was comparable to the natural velocity of motile bacteria. Once contact was established, the two surfaces were pulled apart resulting in retraction data. Figure 12 illustrates the retraction profile for *S. oneidensis* and goethite *versus* diaspore under anaerobic or aerobic conditions (Lower *et al*., 2001a). The intricate details of these curves and the entire data set provide valuable information about intermolecular forces and structures at the bacterium–mineral interface. Initially the entire retraction data were characterized by integrating the force with respect to distance. This provided quantitative energy values associated with adhesion. The retraction curves were further analyzed by the worm-like chain model (see above) to establish a correlation between specific bridging polymers and unique signatures in the retraction curves.

Energy values determined from retraction curves similar to those shown in Lower *et al*. (2001a) revealed that *S. oneidensis* had a higher affinity for diaspore (*versus* goethite) under aerobic conditions (Lower *et al*., 2001a). However, under anaerobic conditions the bacteria exhibited a significant increase in affinity for goethite (see Lower *et al*., 2001a); whereas the adhesion energy for diaspore was indifferent to oxygen concentrations (Lower *et al*., 2001a). The attractive energy between *S. oneidensis* and goethite was 30 aJ (aJ $= 10^{-18}$ J) and 130 aJ under aerobic and anaerobic conditions, respectively. Further, the energetic affinity between goethite and *S. oneidensis* also increased with contact time under

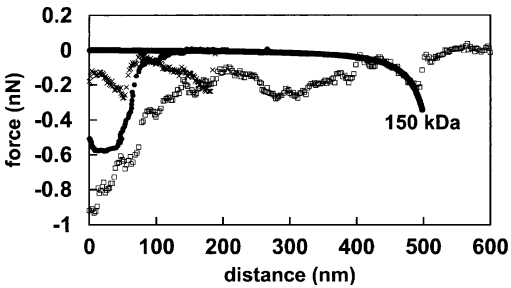

Figure 12 Measured force-distance (or force-extension) relationship between living cells of *S. oneidensis* and diaspore (AlOOH) under anaerobic conditions (solid circles). Interactions with goethite (FeOOH) under aerobic ("X" symbols), or anaerobic conditions (open squares). Also shown is the theoretical prediction for the unravelling of a 150 kDa protein that may tether the bacteria to the surface of goethite (see text). Attractive forces, shown here, have a negative sign. Shown are only those forces measured as the mineral is pulled away from the bacteria (retraction data). Modified from Lower *et al*. (2001a).

anaerobic conditions. This provided quantitative evidence suggesting that this microorganism recognized a particular inorganic surface such that it localized and/or produced biopolymers to mediate contact with goethite under anaerobic conditions.

This idea was further tested by using a "bridging polymer" model to interrogate the intricate details (e.g., the saw-tooth pattern) in the retraction data. As shown above, for the worm-like chain model, linear polymers such as proteins are expected to unravel according to Eq. (4). According to this model, one needs only the persistence length and the contour length to describe the force as a function of the distance a polymer is extended. This model describes a physical process similar to that which is recorded in the retraction data of force microscopy. A protein, for example, in the cell wall of a bacterium makes contact with a mineral. The mineral is then pulled away from the bacterium causing the protein to unravel until it is completely extended at which point the protein is either ripped from the cell wall or it breaks free of the mineral surface and recoils into the cell surface.

The outer surface proteins of *Shewanella* are well characterized. *Shewanella* is known to have proteins on its outer membrane that mediate contact with iron oxyhydroxides (Caccavo, 1999; Caccavo *et al*., 1997; Das and Caccavo, 2000). Several of these proteins are putative iron reductases, which are expected to make physical contact with goethite such that they can transfer electrons across the organic–inorganic interface (Arnold *et al*., 1990; Myers and Nealson, 1990; Myers and Myers, 1992, 1993, 1997; DiChristina and Delong, 1994; Nealson and Saffarini, 1994; Roden and Zachara, 1996; Myers and Myers, 1998, 2000, 2001). In fact, four putative iron reductase proteins have been characterized according to their mass and/or genetic sequence (Myers and Myers, 1997, 1998, 2000, 2001, 2002). The worm-like chain model was used to predict the way in which each of these four proteins (ranging in size from ~50 to 150 kDa; (Myers and Myers, 1997; Myers and Myers, 1998) would unfold. The molecular mass of each protein was used to estimate its overall length according to the following conversion, ~110 Da per amino acid residue (Voet and Voet, 1995). The persistence length of each amino acid, defined as the distance between two adjacent C_α, is equal to 0.38 nm (Karlsson *et al*., 1996; Muller *et al*., 1999; Myers and Myers, 2001). As shown in Fig. 12, the saw-tooth pattern at approximately 500 nm corresponds to the force-extension profile of one of the four putative iron reductase proteins. This profile was reproducible suggesting that the cell wall protein was not ripped from the bacterium, but rather retained its native conformation after multiple extensions. This unique signature was present only for goethite under anaerobic conditions where it was detected in ~80% of the retraction curves, but only when the bacterium was given some period of time to make contact with the surface of goethite (Lower *et al*., 2001a). This suggests that the bacterium required time to "recognize" the mineral surface and subsequently create and/or mobilize a specific protein to the area of contact with goethite.

VI. FUTURE WORK

On Earth, literally millions of different species of prokaryotes may interact with any of the thousands of different minerals. An interface is formed at the junction of a bacterium and a mineral surface that is complex, dynamic, and by its very nature, nanoscale in size. This is because bacteria are living cells that have mastered the art of synthesizing fully functional structures (e.g., lipids, proteins, polysaccharides) and utilizing properties that exist only at the nanometer scale. The study of the interface between minerals and microorganisms requires a unique fusion of geomicrobiology and nanoscale science. What are the fundamental forces that control the binding of a silanol group on a mineral surface to a carboxylic group in a bacterium's cell wall? How does the density and distribution of functional groups on a crystal face influence the way microorganisms sense mineral surfaces? Do bacteria express specific outer surface proteins to interact with certain minerals? How do bacteria modulate forces of interaction between themselves and minerals (or other bacteria) to either enhance or inhibit adhesion and subsequent biofilm formation? Researchers must be able to thoroughly explore both sides of the interface (i.e., the bacterium and the mineral) and the fundamental nanoscale forces in the intervening region to discover phenomena that exist only in the nanospace between a microorganism (or microbially produced polymers) and a mineral surface.

As mentioned earlier, application of force microscopy to the biogeosciences is in its infancy, and there exists many other uses and unexplored possibilities of force experiments with ligands, microorganisms, and minerals. Structural elements within a particular biomolecule/ligand may contribute to its ability to bind to a surface or promote dissolution, or chelate dissolved or mineral bound metals (Stumm, 1992; Ludwig *et al*., 1995; Nubel *et al*., 1996). One can envision collecting a force signature for a large ligand interacting with a mineral, followed by collection of spectra associated with several, individual cognate functional groups associated with the ligand. Comparison of the whole ligand, baseline spectrum with the individual component spectra could reveal which functional groups are dominating the interaction with the mineral. Or, a similar process could be achieved by making force measurements after successive chemical modification of the original ligand structure. Such modification might include inactivation of a specific functional group with a residue-specific reactive reagent (Voet and Voet, 1995), or an amino acid substitution resulting from alteration of the genes associated with the biosynthesis of the molecule. Again changes in the force signature with each modification might help determine the critical moieties contributing to the interaction.

Force maps (Noy *et al*., 1997) are also possible using ligand activated tips. Here, the contrast in the map may be supplied by the differential adhesion between the ligand and various metals that are associated with a surface.

For example, a map constructed with a siderophore activated tip might show large adhesions in areas of high concentrations of trivalent metals such as Fe(III) or Al(III) and lower adhesions for divalent metals such as Cu(II), Zn(II) or Fe(II). Given the spatial resolution of the AFM, such images could be useful for identifying contaminant distribution on a surface or pinpointing impurity concentrations on a mineral growth face, both on a nanometer scale.

CFM is traditionally carried out in a fluid cell (Digital Instruments) that allows direct observation of ligand–surface interaction under environmentally relevant conditions with pico- to nanonewton force resolution and a spatial resolution of tens of nanometers down to potentially the atomic level. Changes in the forces of interaction with solution composition provide important information about the structure and charge character of the ligand and mineral surface, and the nature of the interaction between the two. While the effect of solution composition (e.g. pH) on ligand sorption can be monitored with force measurements using a force titration (Kreller *et al*., 2002). The sensitivity of this technique also allows small changes in mineral solubility and associated metal concentrations, pH, and ionic strength to be detected (Kendall and Hochella, 2003). Given the spatial resolution mentioned above, this opens up the possibility of using this technique to detect localized solution micro- or even nanoenvironments associated with a surface.

Finally, force investigations with living microorganisms are rich with possibilities. For example, one could measure forces of adhesion using wild-type stains *versus* mutants that are incapable of producing specific cell wall macromolecules. These data may result in unique force signatures characteristic of particular biomolecules. Force measurements could also be coupled to other techniques such as confocal scanning laser microscopy. This provides the potential to collect force measurements concurrent with fluorescence observations of the distribution and localization of cell wall macromolecules.

ACKNOWLEDGMENTS

SKL acknowledges the support of the National Science Foundation, the Department of Energy, the American Chemical Society, and the General Research Board of the University of Maryland. SKL would also like to thank J. Tak for support. Funding was provided to TAK by a GAAN Fellowship (U.S. Dept. of Education), the NSF's Nanoscale Science and Engineering (NSE) Program (EAR 01-03053), and the Department of Energy's OBES Geosciences Program (DE-FG02-99ER 15002). TAK acknowledges the support of Michael F. Hochella, Jr. (Virginia Tech).

REFERENCES

Absolom, D. R., Lamberti, F. V., Policova, Z., Zingg, W., van Oss, C. J., and Neumann, A. W. (1983). Surface thermodynamics of bacterial adhesion. *Appl. Environ. Microbiol.* **46**, 90–97.

Albrecht-Gary, A.-M., and Crumbliss, A. L. (1998). Coordination chemistry of siderophores: Thermodynamics and kinetics of iron chelation and release. *In* "Iron transport and storage in microorganisms, plants, and animals" (H. Sigel, Ed.), Vol. 35, pp. 239–327. Marcel Dekker, New York.

Antonik, M. D., D'Costa, N. P., and Hoh, J. H. (1997). A biosensor based on micromechanical interrogation of living cells. *IEEE Engng. Med. Biol.* **16**, 66–72.

Aoki, T., Hiroshima, M., Kitamura, K., Tokunaga, M., and Yanagida, T. (1997). Non-contact scanning probe microscopy with sub-piconewton force sensitivity. *Ultramicroscopy* **70**, 45–55.

Arnold, R. G., Hoffmann, M. R., DiChristina, T. J., and Picardal, F. W. (1990). Regulation of dissimilatory Fe(III) reductase activity in *Shewanella putrefaciens*. *Appl. Environ. Microbiol.* **56**, 2811–2817.

Ashby, P. D., Chen, L., and Lieber, C. M. (2000). Probing intermolecular forces and potentials with magnetic feedback chemical force microscopy. *J. Am. Chem. Soc.* **122**, 9467–9472.

Barker, W. W., Welch, S. A., and Banfield, J. F. (1997). Biogeochemical weathering of silicate minerals. *In* "Geomicrobiology: Interactions Between Microbes and Minerals" (K. H. Nealson, Ed.), Vol. 35, p. 448. Mineralogical Society of America, Washington DC.

Baumgartner, W., Hinterdorfer, P., and Schindler, H. (2000). Data analysis of interaction forces measured with the atomic force microscope. *Ultramicroscopy* **82**, 85–95.

Bell, G. I. (1978). Models for specific adhesion of cell to cells. *Science* **200**, 618–627.

Beveridge, T. J. (1999). Structures of Gram-negative cell walls and their derived membrane vesicles. *J. Bacteriol.* **181**, 4725–4733.

Bhattacharjee, S., Chen, J. Y., and Elimelech, M. (2000). DLVO interaction energy between spheroidal particles and a flat surface. *Colloid. Surf. A: Physicochem. Engng. Aspects* **165**, 143–156.

Bhosle, N., Suci, P. A., Baty, A. M., Weiner, R. M., and Geesey, G. G. (1998). Influence of divalent cations and pH on adsorption of a bacterial polysaccharide adhesion. *J. Colloid. Interf. Sci.* **205**, 89–96.

Binnig, G., Quate, C. F., and Gerber, C. (1986). Atomic force microscope. *Phys. Rev. Lett.* **56**, 930–933.

Bossier, P., Hofte, M., and Verstraete, W. (1988). Ecological Significance of Siderophores in Soil. *In* "Advances in Microbial Ecology" (K. C. Marshall, Ed.), Vol. 10, pp. 385–414. Plenum Press, New York.

Bowen, R. W., Hilal, N., Lovitt, R. W., and Wright, C. W. (1998a). Direct measurement of interactions between adsorbed protein layers using an atomic force microscope. *J. Colloid Interf. Sci.* **197**, 348–352.

Bowen, R. W., Hilal, N., Lovitt, R. W., and Wright, C. W. (1998b). Direct measurement of the force of adhesion of a single biological cell using an atomic force microscopy. *Colloid Surf. A: Physicochem. Engng. Aspects* **136**, 231–234.

Bowen, W. R., Lovitt, R. W., and Wright, C. J. (2000a). Direct quantification of *Aspergillus niger* spore adhesion in liquid using an atomic force microscope. *J. Colloid Interf. Sci.* **228**, 428–433.

Bowen, W. R., Lovitt, R. W., and Wright, C. J. (2000b). Direct quantification of *Aspergillus niger* spore adhesion to mica in air using an atomic force microscope. *Colloid Surf. A-Physicochem. Engng. Aspects* **173**, 205–210.

Brantley, S. L., Liermann, L., and Bau, M. (2001). Uptake of trace metals and rare earth elements from hornblende by a soil bacterium. *Geomicrobiol. J.* **18**, 37–61.

Burnham, N. A., Dominguez, D. D., Mowery, R. L., and Colton, R. J. (1990). Probing the surface forces of monolayer films with an atomic-force microscope. *Phys. Rev. Lett.* **64**, 1931–1934.

Bustamante, C., Marko, J. F., Siggia, E. D., and Smith, S. (1994). Entropic elasticity of lambda-phage DNA. *Science* **265**, 1599–1600.

Butt, H. J., and Jaschke, M. (1995). Calculation of Thermal Noise in Atomic-Force Microscopy. *Nanotechnology* **6**, 1–7.

Butt, H. J., Jaschke, M., and Ducker, W. (1995). Measuring surface forces in aqueous electrolyte solution with the atomic force microscope. *Bioelectrochem. Bioenerg.* **38**, 191–201.

Caccavo, F. (1999). Protein-mediated adhesion of the dissimilatory Fe(III)-reducing bacterium *Shewanella alga* BrY to hydrous ferric oxide. *Appl. Environ. Microbiol.* **65**, 5017–5022.

Caccavo, F. Jr., Schamberger, P. C., Keiding, K., and Nielsen, P. H. (1997). Role of hydrophobicity in adhesion of the dissimilatory Fe(III)-reducing bacterium *Shewanella alga* to amorphous Fe(III) oxide. *Appl. Environ. Microbiol.* **62**, 3837–3843.

Camesano, T. A., and Logan, B. E. (2000). Probing bacterial electrosteric interactions using atomic force microscopy. *Environ. Sci. Technol.* **34**, 3354–3362.

Cappella, B., Baschieri, P., Frediani, C., Miccoli, P., and Ascoli, C. (1997). Force–distance curves by AFM: A powerful technique for studying surface interactions. *IEEE Engng. Med Biol. Mag.* **16**, 58–65.

Cappella, B., and Dietler, G. (1999). Force–distance curves by atomic force microscopy. *Surf. Sci. Rep.* **34**, 1–104.

Cherian, S., and Thundat, T. (2002). Determination of adsorption-induced variation in the spring constant of a microcantilever. *Appl. Phys. Lett.* **80**, 2219–2221.

Cheung, C. L., Hafner, J. H., Chen, L. W., and Lieber, C. M. (2000). Direct growth of single-walled carbon nanotube scanning probe microscopy tips and application to ultrahigh-resolution chemical force microscopy and structural imaging. *Abstr. Pap. Am. Chem. Soc.* **219**, 182.

Chilkoti, A., Boland, T., Ratner, B. D., and Stayton, P. S. (1995). The relationship between ligand-binding thermodynamics and protein–ligand interaction forces measured by atomic force microscopy. *Biophys. J.* **69**, 2125–2130.

Cleveland, J. P., Manne, S., Bocek, D., and Hansma, P. K. (1993). A non-destructive method for determining the spring constant of cantilevers for scanning force microscopy. *Rev. Sci. Instrum.* **64**, 403–405.

Cocozza, C., Tsao, C. C. G., Cheah, S. F., Kraemer, S. M., Raymond, K. N., Miano, T. M., and Sposito, G. (2002). Temperature dependence of goethite dissolution promoted by trihydroxamate siderophores. *Geochimica et Cosmochimica Acta* **66**, 431–438.

Cornell, R. M., and Schwertmann, U. (1996). "The Iron Oxides: Structure, Properties, Reactions, Occurrence and Uses", VCH.

Craig, V. S. J., and Neto, C. (2001). In Situ calibration of colloid probe cantilevers in force microscopy: hydrodynamic drag on a sphere approaching a wall. *Langmuir* **17**, 6018–6022.

Cygan, R. T. (2001). Molecular Modeling in Mineralogy and Geochemistry. *In* "Molecular Modeling Theory: Applications in the Geosciences" (J. D. Kubicki, Ed.), Vol. 42, p. 531. Mineralogical Society of America Geochemical Society, Washington DC.

Dammer, U., Hegner, M., Anselmetti, D., Wagner, P., Dreier, M., Huber, W., and Guentherodt, H. J. (1996). Specific antigen/antibody interactions measured by force microscopy. *Biophys. J.* **70**, 2437–2441.

Dammer, U., Popescu, O., Wagner, P., Anselmetti, D., Guntherodt, H. J., and Misevic, G. N. (1995). Binding Strength Between Cell-Adhesion Proteoglycans Measured By Atomic-Force Microscopy. *Science* **267**, 1173–1175.

Das, A., and Caccavo, F. (2000). Dissimilatory Fe(III) oxide reduction by *Shewnnella alga* BrY requires adhesion. *Curr. Microbiol.* **40**, 344–347.

Davies, D. G., Parsek, M. R., Pearson, J. P., Iglewski, B. H., Costerton, J. W., and Greenberg, E. P. (1998). The involvement of cell-to-cell signals in the development of a bacterial biofilm. *Science* **280**, 295–298.

D'Costa, N. P., and Hoh, J. H. (1995). Calibration of optical lever sensitivity for atomic force microscopy. *Rev. Sci. Instrum.* **66**, 5096–5097.

Degertekin, F. L., Hadimioglu, B., Sulchek, T., and Quate, C. F. (2001). Actuation and characterization of atomic force microscope cantilevers in fluids by acoustic radiation pressure. *Appl. Phys. Lett.* **78**, 1628–1630.

Derjaguin, B. V., and Landau, L. (1941). *Acta Physiochim. URSS* **4**, 633.

Derjaguin, B. V., Muller, V. M., and Toporov, Y. P. (1975). *J. Colloid Interf. Sci.* **53**.

DiChristina, T. J., and Delong, E. F. (1994). Isolation of anaerobic respiratory mutants of *Shewanella putrefaciens* and genetic analysis of mutants deficient in anaerobic growth on Fe^{3+}. *J. Bacteriol.* **176**, 1468–1474.

Ducker, W. A., Senden, T. J., and Pashley, R. M. (1991). Direct measurement of colloidal forces using an atomic force microscope. *Nature* **353**, 239–241.

Ducker, W. A., Senden, T. J., and Pashley, R. M. (1992). Measurement of forces in liquids using a force microscope. *Langmuir* **8**, 1831–1836.

Dziurla, M.-A., Achouak, W., Lam, B.-T., Heulin, T., and Berthelin, J. (1998). Enzyme-linked immunofiltration assay to estimate attachment of Thiobacilli to pyrite. *Appl. Environ. Microbiol.* **64**, 2937–2942.

Edwards, K. J., Schrenk, M. O., Hamers, R., and Banfield, J. F. (1998). Microbial oxidation of pyrite: Experiments using microorganisms from an extreme acidic environment. *Am. Mineral.* **83**, 1444–1453.

Egger, M., Heyn, S.-P., and Gaub, H. E. (1992). Synthetic lipid-anchored receptors based on the binding site of a monoclonal antibody. *Biochim. Biophys. Acta* **1104**, 45–54.

Erlandsson, R., McClelland, G. M., Mate, C. M., and Chiang, S. (1988). Atomic force microscopy using optical interferometry. *J. Vacuum Sci. Technol., A: Vacuum, Surf. Films* **6**, 266–270.

Evans, E. (1999). Energy landscapes of biomolecular adhesion and receptor anchoring at interfaces explored with dynamic force spectroscopy. *Faraday Discussions* **111**, 1–16.

Evans, E. (2001). Probing the relation between force-lifetime and chemistry in single molecular bonds. *Annu. Rev. Biophy. Biomol. Struct.* **30**, 105–128.

Evans, E., and Ipsen, J. (1991). Entropy-driven expansion of electric double layer repulsion between highly flexible membranes. *Electrochim. Acta* **36**, 1735–1741.

Evans, E., and Ludwig, F. (2000). Dynamic strengths of molecular anchoring and material cohesion in fluid biomembranes. *J. Phys.: Condensed Matter* **12**, A315–A320.

Evans, E., and Ritchie, K. (1997). Dynamic strength of molecular adhesion bonds. *Biophysical Journal* **72**, 1541–1555.

Fiorini, M., McKendry, R., Cooper, M. A., Rayment, T., and Abell, C. (2001). Chemical force microscopy with active enzymes. *Biophys. J.* **80**, 2471–2476.

Fleminger, G., and Shabtai, Y. (1995). Direct and rapid analysis of the adhesion of bacteria to solid surfaces: Interaction of fluorescently labeled *Rhodococcus* strain GIN-1 (NCIMB 40340) cells with titanium-rich particles. *Appl. Environ. Microbiol.* **61**, 4357–4361.

Fletcher, M., (Ed.) (1996). "Bacterial Adhesion: Molecular and Ecological Diversity". Wiley-Liss, New York.

Florin, E. L., Moy, V. T., and Gaub, H. E. (1994). Adhesion Forces Between Individual Ligand–Receptor Pairs. *Science* **264**, 415–417.

Flory, P. J. (1989). "Statistical Mechanics of Chain Molecules". Hanser Publishers, Munich.

Fortin, D., Ferris, F. G., and Beveridge, T. J. (1997). Surface-mediated mineral development by bacteria. *In* "Geomicrobiology: Interactions between Microbes and Minerals" (K. H. Nealson, Ed.), Vol. 35, pp. 161–180. Mineralogical Society of America, Washington DC.

Frisbie, C. D., Rozsnyai, L. F., Noy, A., Wrighton, M. S., and Lieber, C. M. (1994). Functional-group imaging by chemical force microscopy. *Science* **265**, 2071–2074.

Gay, C., and Leibler, L. (1999). On stickiness. *Phys. Today* **52**, 48–52.

Gergely, C., Hemmerle, J., Schaaf, P., Horber, J. K. H., Voegel, J.-C., and Senger, B. (2002). Multi-bead-and-spring model to interpret protein detachment studied by AFM force spectroscopy. *Biophys. J.* **83**, 706–722.

Gergely, C., Senger, B., Voegel, J. C., Horber, J. K. H., Schaaf, P., and Hemmerle, J. (2001). Semi-automatized processing of AFM force-spectroscopy data. *Ultramicroscopy* **87**, 67–78.

Gibson, C. T., Weeks, B. L., Lee, J. R. I., Abell, C., and Rayment, T. (2001). A nondestructive technique for determining the spring constant of atomic force microscope cantilevers. *Rev. Sci. Instrum.* **72**, 2340–2343.

Goddenhenrich, T., Lemke, H., Hartmann, U., and Heiden, C. (1990). Force microscope with capacitive displacement detection. *J. Vacuum Sci. Technol., A: Vacuum, Surf., Films* **8**, 383–387.

Grabarek, Z., and Gergely, J. (1990). Zero-length crosslinking procedure with the use of active esters. *Anal. Biochem.* **185**, 131–135.

Grandbois, M., Beyer, M., Rief, M., Clausen-Schaumann, H., and Gaub, H. E. (1999). How strong is a covalent bond? *Science* **283**, 1727–1730.

Grubmuller, H., Heymann, B., and Tavan, P. (1996). Ligand binding: molecular mechanics calculation of the streptavidin–biotin rupture force. *Science* **271**, 997–999.

Hafner, J. H., Cheung, C. L., and Lieber, C. M. (1999). Growth of nanotubes for probe microscopy tips. *Nature* **398**, 761–762.

Hafner, J. H., Cheung, C. L., Woolley, A. T., and Lieber, C. M. (2001). Structural and functional imaging with carbon nanotube AFM probes. *Progress in Biophys. & Molec. Biol.* **77**, 73–110.

Han, T., Williams, J. M., and Beebe, T. P. (1995). Chemical-bonds studied with functionalized atomic-force microscopy tips. *Analytical Chemica Acta* **307**, 365–376.

Hansen, D. C., McCafferty, E., Lins, C. W., and Fitzpatrick, J. J. (1995). An FT-IR investigation of parabactin adsorbed onto aluminium. *Appl. Surf. Sci.* **84**, 85–90.

Hartmann, U. (1991). van der Waals interactions between sharp probes and flat sample surfaces. *Phys. Rev. B* **43**, 2404–2407.

Heinz, W. F., and Hoh, J. H. (1999). Spatially resolved force spectroscopy of biological surfaces using the atomic force microscope. *Trends Biotechnol.* **17**, 143–150.

Hersman, L. E. (2000). The role of siderophores in iron oxide dissolution. *In* "Environmental microbe-metal interactions" (D. R. Lovley, Ed.), p. 395. ASM Press, Washington DC.

Hersman, L., Lloyd, T., and Sposito, G. (1995). Siderophore-promoted dissolution of hematite. *Geochim. Cosmochim. Acta* **59**, 3327–3330.

Hiebert, F. K., and Bennett, P. C. (1992). Microbial control of silicate weathering in organic-rich ground water. *Science* **258**, 278–281.

Hinterdorfer, P., Baumgartner, W., Gruber, H. J., Schilcher, K., and Schindler, H. (1996). Detection and localization of individual antibody-antigen recognition events by atomic force microscopy. *Proc. Natl. Acad. Sci. USA* **93**, 3477–3481.

Hinterdorfer, P., Gruber, H. J., Kienberger, F., Kada, G., Riener, C., Borken, C., and Schindler, H. (2002). Surface attachment of ligands and receptors for molecular recognition force microscopy. *Colloid Surf., B: Biointerf.* **23**, 115–123.

Holmen, B. A., and Casey, W. H. (1996). Hydroxamate ligands, surface chemistry, and the mechanism of ligand-promoted dissolution of goethite [α-FeOOH(s)]. *Geochim. Cosmochim. Acta* **22**, 4403–4416.

Holmen, B. A., Tejedor-Tejedor, M. I., and Casey, W. H. (1997). Hydroxamate complexes in solution and at the goethite-water interface: a cylindrical internal reflection fourier transform infrared spectroscopy study. *Langmuir* **13**, 2197–2206.

Hutter, J. L., and Bechhoefer, J. (1993). Calibration of atomic-force microscope tips. *Rev. Sci. Instrum.* **64**, 1868–1873.

Israelachvili, J. N. (1992). "Intermolecular and Surface Forces", 2nd edn. Academic Press, San Diego.

Israelachvili, J. N., and McGuiggan, P. M. (1988). Forces between surfaces in liquids. *Science* **241**, 795–800.

Ito, T., Citterio, D., Buehlmann, P., and Umezawa, Y. (1999). Observation of silver and hydrogen ion binding to self-assembled monolayers using chemically modified AFM tips. *Langmuir* **15**, 2788–2793.

Izrailev, S., Stepaniants, S., Balsera, M., Oono, Y., and Schulten, K. (1997). Molecular dynamics study of unbinding of the avidin–biotin complex. *Biophys. J.* **72**, 1568–1581.

Jarvis, S. P., Duerig, U., Lantz, M. A., Yamada, H., and Tokumoto, H. (1998). Feedback-stabilized force sensors. A gateway to the direct measurement of interaction potentials. *Appl. Phys. A: Mater. Sci. Process.* **A66**, S211–S213.

Jarvis, S. P., Yamada, H., Yamamoto, S. I., Tokumoto, H., and Pethica, J. B. (1996). Direct mechanical measurement of interatomic potentials. *Nature (London)* **384**, 247–249.

Jeppesen, C., Wong, J. Y., Kuhl, T. L., Israelachvili, J., Mullah, J. N., Zalipsky, S., and Marques, C. M. (2001). Impact of polymer tether length on multiple ligand–receptor bond formation. *Science* **293**, 465–468.

Jericho, S. K., and Jericho, M. H. (2002). Device for the determination of spring constants of atomic force microscope cantilever and micromachined springs. *Rev. Sci. Instrum.* **73**, 2483–2485.

Johnson, K. L., Kendall, K., and Roberts, A. D. (1971). Surface energy and the contact of elastic solids. *Proc. R. Soc. Lond. A* **324**, 301–313.

Joyce, S. A., and Houston, J. E. (1991). A new force sensor incorporating force-feedback control for interfacial force microscopy. *Rev. Sci. Instrum.* **62**, 710–715.

Kalinowski, B. E., Liermann, L. J., Brantley, S. L., Barnes, A., and Pantano, C. G. (2000). X-ray photoelectron evidence for bacteria-enhanced dissolution of hornblende. *Geochim. Cosmochim. Acta* **64**, 1331–1343.

Karlsson, J.-J., Kadziola, A., Rasmussen, A., Rostrup, T. E., and Ulstrup, J. (1996). Electron transfer of the di-heme protein: *Pseudomonas stutzeri* cytochrome c_4. *In* "Protein Folds: A Distance-Based Approach" (S. Brunak, Ed.), pp. 56–67. CRC Press, Boca Raton.

Kasas, S., Riederer, B. M., Catsicas, S., Cappella, B., and Dietler, G. (2000). Fuzzy logic algorithm to extract specific interaction forces from atomic force microscopy data. *Rev. Sci. Instrum.* **71**, 2082–2086.

Kendall, K. (1994). Adhesion: Molecules and mechanics. *Science* **263**, 1720–1725.

Kendall, T. A., and Hochella, M. F. Jr. (2003). The measurement and interpretation of molecular level forces of interaction between the siderophore azotobactin and mineral surfaces. *Geochim. Cosmochim. Acta.*

Kienberger, F., Kada, G., Gruber, H. J., Pastushenko, V. P., Riener, C., Trieb, M., Knaus, H.-G., Schindler, H., and Hinterdorfer, P. (2000). Recognition force spectroscopy studies of the NTA-His6 bond. *Single Mol.* **1**, 59–65.

Kosmulski, M. (2001). "Chemical properties of material surfaces". Marcel Dekker, New York.

Kraemer, S. M., Cheah, S. F., Zapf, R., Xu, J. D., Raymond, K. N., and Sposito, G. (1999). Effect of hydroxamate siderophores on Fe release and Pb(II) adsorption by goethite. *Geochim. Cosmochim. Acta* **63**, 3003–3008.

Kraemer, S. M., Xu, J. D., Raymond, K. N., and Sposito, G. (2002). Adsorption of Pb(II) and Eu(III) by oxide minerals in the presence of natural and synthetic hydroxamate siderophores. *Environ. Sci. Technol.* **36**, 1287–1291.

Kreller, D. I., Gibson, G., van Loon, G. W., and Horton, J. H. (2002). Chemical Force Microscopy Investigation of Phosphate Adsorption on the Surfaces of Iron(III) Oxyhydroxide Particles. *J. Colloid Interf. Sci.* **254**, 205–213.

Kummert, R., and Stumm, W. (1980). The surface complexation of organic acids on hydrous.gamma. alumina. *J. Colloid Interf. Sci.* **75**, 373–385.

Lawrence, J. R., Korber, D. R., Hoyle, B. D., Costerton, J. W., and Caldwell, D. E. (1991). Optical sectioning of microbial biofilms. *J. Bacteriol.* **173**, 6558–6567.

Leckband, D., and Israelachvili, J. (2001). Intermolecular forces in biology. *Q. Rev. Biophy.* **34**, 105–267.

Lee, G. U., Chrisey, L. A., and Colton, R. J. (1994a). Direct Measurement of the Forces between Complementary Strands of DNA. *Science* **266**, 771–773.

Lee, G. U., Kidwell, D. A., and Colton, R. J. (1994b). Sensing discrete streptavidin–biotin interactions with atomic force microscopy. *Langmuir* **10**, 354–357.

Liermann, L. J., Kalinowski, B. E., Brantley, S. L., and Ferry, J. G. (2000). Role of bacterial siderophores in dissolution of hornblende. *Geochim. Cosmochim. Acta* **64**, 587–602.

Lo, Y. S., Huefner, N. D., Chan, W. S., Stevens, F., Harris, J. M., and Beebe, T. P. (1999). Specific interactions between biotin and avidin studied by atomic force microscopy using the Poisson statistical analysis method. *Langmuir* **15**, 1373–1382.

Lo, Y. S., Simons, J., and Beebe, T. P. (2002). Temperature dependence of the biotin–avidin bond-rupture force studied by atomic force microscopy. *Journal of Physical Chemistry B* **106**, 9847–9852.

Lower, S. K., Tadanier, C. J., and Hochella, M. F. (2000). Measuring interfacial and adhesion forces between bacteria and mineral surfaces with biological force microscopy. *Geochim. Cosmochim. Acta* **64**, 3133–3139.

Lower, S. K., Hochella, M. F., and Beveridge, T. J. (2001a). Bacterial recognition of mineral surfaces: Nanoscale interactions between *Shewanella* and α-FeOOH. *Science* **292**, 1360–1363.

Lower, S. K., Tadanier, C. J., and Hochella, M. F. (2001b). Dynamics of the mineral-microbe interface: Use of biological force microscopy in biogeochemistry and geomicrobiology. *Geomicrobiol. J.* **18**, 63–76.

Lower, S. K., Hochella, M. F. Jr., Banfield, J. F., and Rosso, K. (2002). Nanogeoscience: From the movement of electrons to lithosphere plates. *Eos: Trans. Am. Geophys. Union* **83**, 53–56.

Ludwig, C., Casey, W. H., and Rock, P. A. (1995). Prediction of ligand-promoted dissolution rates from the reactivities of aqueous complexes. *Nature (London)* **375**, 44–47.

Maeda, N., and Senden, T. J. (2000). A Method for the Calibration of Force Microscopy Cantilevers via Hydrodynamic Drag. *Langmuir* **16**, 9282–9286.

Marszalek, P. E., Oberhauser, A. F., Pang, Y. -P., and Fernandez, J. M. (1998). Polysaccharide elasticity governed by chair-boat transitions of the glucopyranose ring. *Nature (London)* **396**, 661–664.

Maurice, P. A., Lee, Y. J., and Hersman, L. E. (2000). Dissolution of Al-substituted goethites by an aerobic *Pseudomonas mendocina* var. bacteria. *Geochim Cosmochim Acta* **64**, 1363–1374.

Mazzola, L. T., Frank, C. W., Fodor, S. P. A., Mosher, C., Lartius, R., and Henderson, E. (1999). Discrimination of DNA hybridization using chemical force microscopy. *Biophys. J.* **76**, 2922–2933.

Merkel, R., Nassoy, P., Leung, A., Ritchie, K., and Evans, E. (1999). Energy landscapes of receptor-ligand bonds explored with dynamic force spectroscopy. *Nature* **397**, 50–53.

Meyer, G., and Amer, N. M. (1990). Simultaneous measurement of lateral and normal forces with an optical-beam-deflection atomic force microscope. *Appl. Phys. Lett.* **57**, 2089–2091.

Moy, V. T., Florin, E. L., and Gaub, H. E. (1994a). Intermolecular forces and energies between ligands and receptors. *Science* **266**, 257–259.

Moy, V. T., Florin, E.-L., and Gaub, H. E. (1994b). Adhesive forces between ligand and receptor measured by AFM. *Colloid Surf., A: Physicochem. Engng. Aspects* **93**, 343–348.

Muller, D. J., and Engel, A. (1997). The height of biomolecules measured with the atomic force microscope depends on electrostatic interactions. *Biophy. J.* **73**, 1633–1644.

Muller, D. J., Baumeister, W., and Engel, A. (1999). Controlled unzipping of a bacterial surface layer with atomic force microscopy. *Proc. Nat. Acad. Sci. USA* **96**, 13170–13174.

Myers, C. R., and Nealson, K. H. (1988). Bacterial manganese reduction and growth with manganese oxide as the sole electron acceptor. *Science* **240**, 1319–1321.

Myers, C. R., and Nealson, K. H. (1990). Respiration-linked proton translocation coupled to anaerobic reduction of manganese(IV) and iron(III) in *Shewanella putrefaciens* MR-1. *J. Bacteriol.* **172**, 6232–6238.

Myers, C. R., and Myers, J. M. (1992). Localization of cytochromes to the outer membrane of anaerobically grown. *Shewanella putrefaciens* MR-1. *J. Bacteriol.* **174**, 3429–3438.

Myers, C. R., and Myers, J. M. (1993). Ferric reductase is associated with the membranes of anaerobically grown *Shewanella putrefaciens* MR-1. *Fems Microbiol. Lett.* **108**, 15–22.

Myers, C. R., and Myers, J. M. (1997). Outer membrane cytochromes of *Shewanella putrefaciens* MR-1: Spectral analysis, and purification of the 83-kDa *c*-type cytochrome. *Biochim. Biophys. Acta* **1326**, 307–318.

Myers, J. M., and Myers, C. R. (1998). Isolation and sequence of *omcA*, a gene encoding a decaheme outer membrane cytochrome *c* of *Shewanella putrefaciens* MR-1, and detection of *omcA* homologs in other strains of *S. putrefaciens*. *Biochim. Biophys. Acta* **1373**, 237–251.

Myers, J. M., and Myers, C. R. (2000). Role of the tetraheme cytochrome CymA in anaerobic electron transport in cells of *Shewanella putrefaciens* MR-1 with normal levels of menaquinone. *J. Bacteriol.* **182**, 67–75.

Myers, J. M., and Myers, C. R. (2001). Role for outer membrane cytochromes OmcA and OmcB of *Shewanella putrefaciens* MR-1 in reduction of manganese dioxide. *Appl. Environ. Microbiol.* **67**, 260–269.

Myers, J. M., and Myers, C. R. (2002). Genetic complementation of an outer membrane cytochrome omcB mutant of *Shewanella putrefaciens* MR-1 requires omcB plus downstream DNA. *Appl. Environ. Microbiol.* **68**, 2781–2793.

Nealson, K. H., and Saffarini, D. (1994). Iron and manganese in anaerobic respiration: Environmental significance, physiology, and regulation. *Ann. Rev. Microbiol.* **48**, 311–343.

Neubauer, U., Nowack, B., Furrer, G., and Schulin, R. (2000). Heavy metal sorption on clay minerals affected by the siderophore desferrioxamine B. *Environ. Sci. Technol.* **34**, 2749–2755.

Noy, A., Vezenov, D. V., and Lieber, C. M. (1997). Chemical force microscopy. *Ann. Rev. Mater. Sci.* **27**, 381–421.

Nubel, U., Engelen, B., Felske, A., Snaidr, J., Wieshuber, A., Amann, R. I., Ludwig, W., and Backhaus, H. (1996). Sequence heterogeneities of genes encoding 16S rRNAs in *Paenibacillus polymyxa* detected by temperature gradient gel electrophoresis. *J. Bacteriol.* **178**, 5636–5643.

Ohmura, N., Kitamura, K., and Saiki, H. (1993). Selective adhesion of *Thiobacillus ferrooxidans* to pyrite. *Appl. Environ. Microbiol.* **59**, 4044–4050.

Ong, Y.-L., Razatos, A., Georgiou, G., and Sharma, M. M. (1999). Adhesion forces between *E. coli* bacteria and biomaterial surfaces. *Langmuir* **15**, 2719–2725.

Oreskes, N., Shrader-Frechette, K., and Belitz, K. (1994). Verification, validation, and confirmation of numerical models in the Earth Sciences. *Science* **263**, 641–646.

Pleuddemann, E. P. (1991). "Silane Coupling Agents". Plenum Press, New York.

Rabinovich, Y. I., and Yoon, R. H. (1994). Use of atomic force microscope for the measurements of hydrophobic forces between silanated silica plate and glass sphere. *Langmuir* **10**, 1903–1909.

Razatos, A., Ong, Y. L., Sharma, M. M., and Georgiou, G. (1998a). Evaluating the interaction of bacteria with biomaterials using atomic force microscopy. *J. Biomater. Sci. Polym. Edu.* **9**, 1361–1373.

Razatos, A., Ong, Y.-L., Sharma, M. M., and Georgiou, G. (1998b). Molecular determinants of bacterial adhesion monitored by atomic force microscopy. *Proc. Nat. Acad. Sci. USA* **95**, 11059–11064.

Rezania, A., Johnson, R., Lefkow, A., and Healy, K. E. (1999). Bioactivation of metal oxide surfaces. 1. Surface characterization and cell response. *Langmuir* **15**, 6931–6939.

Rief, M., Gautel, M., Oesterhelt, F., Fernandez, J. M., and Gaub, H. E. (1997a). Reversible unfolding of individual titin immunoglobulin domains by AFM. *Science (Washington, D.C.)* **276**, 1109–1112.

Rief, M., Oesterhelt, F., Heymann, B., and Gaub, H. E. (1997b). Single molecule force spectroscopy on polysaccharides by atomic force microscopy. *Science (Washington, D.C.)* **275**, 1295–1297.

Roden, E. E., and Zachara, J. M. (1996). Microbial reduction of crystalline iron(III) oxides: Influence of oxide surface area and potential for cell growth. *Environ. Sci. Technol.* **30**, 1618–1628.

Rugar, D., Mamin, H. J., and Guethner, P. (1989). Improved fiber-optic interferometer for atomic force microscopy. *Appl. Phys. Lett.* **55**, 2588–2590.

Ryan, J. N., and Gschwend, P. M. (1994). Effects of ionic-strength and flow-rate on colloid release — relating kinetics to intersurface potential-energy. *J. of Colloid and Interface Science* **164**, 21–34.

Ryan, J. N., and Elimelech, M. (1996). Colloid mobilization and transport in groundwater. *Colloid Surf. a-Physicochem. Eng. Aspects* **107**, 1–56.

Sader, J. E., and White, L. (1993). Theoretical analysis of the static deflection of plates for atomic force microscope applications. *J. Appl. Phys.* **74**, 1–9.

Sader, J. E., Larson, I., Mulvaney, P., and White, L. R. (1995). Method for the calibration of atomic force microscope cantilevers. *Rev. Sci. Instrum.* **66**, 3789–3798.

Sader, J. E. (1998). Frequency response of cantilever beams immersed in viscous fluids with applications to the atomic force microscope. *J. Appl. Phys.* **84**, 64–76.

Sader, J. E., Chon, J. W. M., and Mulvaney, P. (1999). Calibration of rectangular atomic force microscope cantilevers. *Rev. Sci. Instrum.* **70**, 3967–3969.

Schmitt, L., Ludwig, M., Gaub, H. E., and Tampe, R. (2000). A metal-chelating microscopy tip as a new toolbox for single-molecule experiments by atomic force microscopy. *Biophy. J.* **78**, 3275–3285.

Schultze-Lam, S., Harauz, G., and Beveridge, T. J. (1992). Participation of a cyanobacterial S-layer in fine-grain mineral formation. *J. Bacteriol.* **174**, 7971–7981.

Schwesinger, F., Ros, R., Strunz, T., Anselmetti, D., Guntherodt, H. J., Honegger, A., Jermutus, L., Tiefenauer, L., and Pluckthun, A. (2000). Unbinding forces of single antibody-antigen complexes correlate with their thermal dissociation rates. *Proc. Nat. Acad. Sci. USA* **97**, 9972–9977.

Seaman, J. C., Alexander, D. B., Loeppert, R. H., and Zuberer, D. A. (1992). The availability of iron from various solid-phase iron sources to a siderophore producing pseudomonas strain. *J. Plant Nutr.* **15**, 2221–2233.

Sposito, G. (1989). "The Chemistry of Soils". Oxford University Press, New York.

Stevens, F., Lo, Y. S., Harris, J. M., and Beebe, T. P. (1999). Computer modeling of atomic force microscopy force measurements: Comparisons of Poisson, histogram, and continuum methods. *Langmuir* **15**, 207–213.

Stone, A. T. (1997). Reactions of extracellular organic ligands with dissolved metal ions and mineral surface. "Geomicrobiology: Interactions Between Microbes and Minerals" (K. H. Nealson, Ed.), Vol. 35, pp. 309–341. Mineralogical Society of America, Washington D.C.

Strunz, T., Oroszlan, K., Schafer, R., and Guntherodt, H.-J. (1999). Dynamic force spectroscopy of single DNA molecules. *Proc. Nat. Acad. Sci. USA* **96**, 11277–11282.

Stumm, W. (1992). "Chemistry of the Solid-Water Interface". Wiley, Inc., New York.

Swamy, M. J. (1995). Thermodynamic analysis of biotin binding to avidin. A high sensitivity titration calorimetric study. *Biochem. Mol. Biol. Int.* **36**, 219–225.

Telford, J. R., and Raymond, K. N. (1996). Siderophores. *Compr. Supramol. Chem.* **1**, 245–266.

Toikka, G., Hayes, R. A., and Ralston, J. (1996). Surface forces between spherical ZnS particles in aqueous electrolyte. *Langmuir* **12**, 3783–3788.

Tokunaga, M., Aoki, T., Hiroshima, M., Kitamura, K., and Yanagida, T. (1997). Subpiconewton intermolecular force microscopy. *Biochem. Biophys. Res. Commun.* **231**, 566–569.

Torii, A., Sasaki, M., Hane, K., and Okuma, S. (1996). A method for determining the spring constant of cantilevers for atomic force microscopy. *Meas. Sci. Technol.* **7**, 179–184.

van Loosdrecht, M. C. M., Lyklema, J., Norde, W., and Zehnder, A. J. B. (1989). Bacterial adhesion: A physicochemical approach. *Microbial. Ecol.* **17**, 1–15.

van Oss, C. J. (1993). Acid-base interfacial interactions in aqueous media. *Colloid Surf. A: Physicochem. Engg. Aspects* **78**, 1–49.

Verwey, E. J., and Overbeek, J. T. G. (1948). "Theory of the Stability of Lyophobic Colloids". Elsevier Publishing, Amsterdam.

Vigeant, M. A.-S., Ford, R. M., Wagner, M., and Tamm, L. K. (2002). Reversible and irreversible adhesion of motile *Escherichia coli* cells analyzed by total internal reflection aqueous fluorescence microscopy. *Appl. Environ. Microbiol.* **68**, 2794–2801.

Voet, D., and Voet, J. (1995). "Biochemistry", 2nd edn. John Wiley & Sons, New York.

Wagner, P. (1998). Immobilization strategies for biological scanning probe microscopy. *FEBS Lett.* **430**, 112–115.

Watteau, F., and Berthelin, J. (1994). Microbial dissolution of iron and aluminum from soil minerals — efficiency and specificity of hydroxamate siderophores compared to aliphatic-acids. *Eur. J. Soil Biol.* **30**, 1–9.

Weisenhorn, A. L., Maivald, P., Butt, H. J., and Hansma, P. K. (1992). Measuring Adhesion, Attraction, and Repulsion Between Surfaces in Liquids With an Atomic-Force Microscope. *Phys. Rev. B* **45**, 11226–11232.

Wenzler, L. A., Moyes, G. L., Olson, L. G., Harris, J. M., and Beebe, T. P. (1997). Single molecule bond-rupture force analysis of interactions between AFM tips and substrates modified with organosilanes. *Analytical Chemistry* **69**, 2855–2861.

Whitman, W. B., Coleman, D. C., and Wiebe, W. J. (1998). Prokaryotes: The unseen majority. *Proc. Nat. Acad. Sci. USA.* **95**, 6578–6583.

Williams, J. M., Han, T. J., and Beebe, T. P. (1996). Determination of single-bond forces from contact force variances in atomic force microscopy. *Langmuir* **12**, 1291–1295.

G. Winkelmann, (Ed.), (1991). *In* "CRC Handbook of Microbial Iron Chelates" CRC Press, Boca Raton, Florida.

Wong, S. S., Joselevich, E., Wooley, A. T., Cheung, C. L., and Lieber, C. M. (1998a). Covalently functionalized nanotubes as nanometre-sized probes in chemistry and biology. *Nature* **394**, 52–55.

Wong, S. S., Woolley, A. T., Joselevich, E., Cheung, C. L., and Lieber, C. M. (1998b). Covalently-functionalized single-walled carbon nanotube probe tips for chemical force microscopy. *J. of American Chemical Society* **120**, 8557–8558.

Wong, J., Chilkoti, A., and Moy, V. T. (1999). Direct force measurements of the streptavidin–biotin interaction. *Biomol. Engg.* **16**, 45–55.

Yamamoto, S.-i., Yamada, H., and Tokumoto, H. (1997). Precise force curve detection system with a cantilever controlled by magnetic force feedback. *Rev. Sci. Instrum.* **68**, 4132–4136.

Yao, H.-L., and Yeh, H.-H. (1996). Fumarate, Maleate, and Succinate Adsorption on Hydrous.delta.-A12O3. 1. Comparison of the Adsorption Maxima and Their Significance. *Langmuir* **12**, 2981–2988.